Dynamic tipping in the non-smooth Stommel-box model, with fast oscillatory forcing.

Chris Budd * Cody Griffith † Rachel Kuske ‡

June 7, 2021

Abstract

We study the behaviour at tipping points close to non-smooth fold bifurcations in non-autonomous systems. The focus is the Stommel-Box, and related climate models, which are piecewise-smooth continuous dynamical systems, modelling thermohaline circulation. We obtain explicit asymptotic expressions for the behaviour at tipping points in the settings of both slowly varying freshwater forcing and rapidly oscillatory fluctuations. The results, based on combined multiple scale and local analyses, provide conditions for the sudden transitions between temperature-dominated and salinity-dominated states. In the context of high frequency oscillations, a multiple scale averaging approach can be used instead of the usual geometric approach normally required for piecewise-smooth continuous systems. The explicit parametric dependencies of advances and lags in the tipping show a competition between dynamic features of the model. We make a contrast between the behaviour of tipping points close to both smooth Saddle Node Bifurcations and the non-smooth systems studied on this paper. In particular we show that the non-smooth case has earlier and more abrupt transitions. This result has clear implications for the design of early warning signals for tipping in the case of the non-smooth dynamical systems which often arise in climate models.

Keywords: Non-smooth dynamics, conceptual climate models, dynamic bifurcation, tipping, multiple scales, border collision, non-autonomous systems.

1 Introduction

1.1 Overview

Various models of phenomena in climate have been used both to model and to predict abrupt changes in systems with a wide range of time-scales. As a result, there are many climate models that include non-smooth features approximating transitions over short times relative to climate time-scales. These include state-dependent switches, non-smooth functional descriptions of dynamics, and discrete states delineated by boundaries. Examples of these are given by: the PP04 model of sudden changes in carbon dioxide emission rates during glacial cycles [13], [12], rainfall [9], and the motion of the ice fronts in a glacial cycle [19], as well as the Stommel box model for thermohaline circulation that we study in this paper. In all such systems we see both the dynamics commonly found in smooth systems (such as possibly co-existing periodic and chaotic states and transitions between them including tipping points), as well as dynamical behaviors specific to non-smooth

*Dept. of Mathematical Sciences, University of Bath, UK
†University of British Columbia, UBC, present affiliation: 908devices
‡School of Mathematics, Georgia Institute of Technology, Atlanta, USA.

systems, such as grazing, sliding, and non-smooth bifurcations between different co-existing states [3].

Transitions in the context of bi-stability have been studied in many contexts. A common setting is where stability is lost via bifurcations, and the system experiences hysteresis as parameters vary through these critical points, depending upon the form of the parameter variation. For these non-autonomous systems with varying parameters the transitions between states may be qualitatively different, depending on the nonlinearities, the types of underlying static bifurcations, and the vector fields near the stable equilibria.

Throughout this paper we use the term *tipping* to refer to a sudden transition from one qualitatively different state to another in the non-autonomous setting. We note the contrast with a bifurcation, a qualitative change in the geometry of a system in which its flow or phase portrait is altered in the dynamical context. Tipping is used in a wider variety of settings, generically a qualitative change in behaviour along a particular time-varying trajectory. The two are sometimes related, as tipping may be related to a bifurcation point or some other separatrix of a particular object in the flow, such as a fold point of a slow manifold or stable manifold of a saddle. This relationship is indeed present in the systems we study here: the non-autonomous systems with time-varying parameters have autonomous counterparts with static parameters treated as bifurcation parameters. Given this connection, we use the term dynamic bifurcation to refer to the specific setting where a parameter value varies in time near or through the critical value of a static bifurcation parameter from an underlying autonomous system.

In this paper we focus on the dynamic transitions near Non-Smooth Fold (NSF) bifurcations, obtaining explicit results that can be contrasted with analogous transitions near smooth Saddle-Node Bifurcations (SNBs) [20]. We obtain explicit asymptotic expressions for the tipping points in the Stommel Box climate model. In particular we find conditions for sudden transitions between temperature-dominated and salinity-dominated states. We look at time variation which is a combination of a slow change in the mean parameter value combined with a rapidly oscillating (seasonal) perturbation, and determine when these lead to rapid transitions between qualitatively different states. From the comparisons with the tipping points in smooth systems [20], there are clear implications for the development of early warning signals, given the close connection with the dynamics of the underlying reduced system [10], [7]. Specifically we show that tipping occurs earlier, and more abruptly in the non-smooth model. This is because in the non-smooth case the eigenvalues associated with the linearisation about the fixed points do not drop to zero at the tipping point and hence, unlike the smooth case, they do not generate a warning signal that tipping is likely to occur.

1.2 The Stommel Box model

A well-known class of models, where salinity-dominated and temperature-dominated states are bi-stable, is that of thermohaline circulation (THC). Here abrupt qualitative changes are possible, see Alley [1], Marotzke [11], or Rahmstorf [14] and [15]. Recently Rahmstorf was able to find evidence of weakening occurring around these abrupt changes in a system of ocean patterns known as the Atlantic meridional overturning circulation (AMOC) [4]. This evidence of ocean dynamics responding to changes in surface temperature underscores the need to understand the transitions in these types of systems. We note that such transitions can be either smooth or non-smooth (as described in [3]). In this paper we focus on the commonly used Stommel two box model [18] as an exemplar for studying the transitions in the THC (or more generally, the dynamical impact of NSF bifurcations between equilibrium states) in a realistic climate model. We begin with the non-dimensionalized Stommel model as given in [5],

$$\begin{aligned} \dot{\mathcal{T}} &= \eta_1 - \mathcal{T}(1 + |\mathcal{T} - \mathcal{S}|), \\ \dot{\mathcal{S}} &= \eta_2 - \mathcal{S}(\eta_3 + |\mathcal{T} - \mathcal{S}|). \end{aligned} \tag{1.1}$$

The variables $\mathcal{T}$ and $\mathcal{S}$ are the dimensionless equatorial-to-pole differences for temperature and salinity, respectively. The parameters η_1, η_2, and η_3 are also dimensionless quantities, with η_1 representing thermal variation, η_2 as the freshwater flux, and η_3 as the ratio of relaxation times of temperature and salinity. The dimensionless AMOC strength is captured by the difference

$$\mathcal{V} = \mathcal{T} - \mathcal{S},$$

which plays an important role throughout the dynamical analysis. With the dependence on the absolute value $|\mathcal{T} - \mathcal{S}|$, (1.1) is a non-smooth dynamical system. It has a discontinuity surface at

$$\Sigma = \{(\mathcal{T}, \mathcal{S}) : \mathcal{T} - \mathcal{S} \equiv \mathcal{V} = 0\}. \tag{1.2}$$

The equations for $\mathcal{T}$ and $\mathcal{S}$ then describe different dynamics in Σ^+ and Σ^- for

$$\Sigma^+ = \{(\mathcal{T}, \mathcal{S}) : \mathcal{T} - \mathcal{S} > 0\} \qquad \Sigma^- = \{(\mathcal{T}, \mathcal{S}) : \mathcal{T} - \mathcal{S} < 0\}. \tag{1.3}$$

The model is non-smooth through the action of the nonlinearity $|\mathcal{T} - \mathcal{S}|$ and takes the form of a *piecewise-smooth continuous system* with a degree of discontinuity of 2 [3], [17].

A standard analysis of the static model, where typically η_1 and η_3 are fixed, and η_2 is treated as a bifurcation parameter, yields stability regions for the temperature and stability dominated states. Taking values of η_1 and η_3 as is usual in applications [5], there are either 3 or 1 fixed points. In the case of 3 fixed points, we identify two different critical points, denoted η_{2sf} and η_{2c} with $\eta_{2sf} > \eta_{2c}$. For $\eta_{2sf} > \eta_2 > \eta_{2c}$, there are two fixed points in Σ^+ which are a saddle (**S**) and a stable node (**N**), which loses stability at the (smooth) SNB η_{2sf}. Further for $\eta_2 > \eta_{2c}$ in Σ^- there is a fixed point which is a stable focus (**F**). If $\eta_2 < \eta_{2c}$ there is a single stable node **N** in Σ^+. These are illustrated in Figure 1 for $\mathcal{V}$ vs. η_2. Note that **N** corresponds to the temperature-dominated state, and **F** corresponds to the salinity-dominated state.

The critical point η_{2c}, indicated by $*$ in Figure 1 corresponds to a *border collision bifurcation* (BCB) arising when **F** and **S** intersect with Σ. This critical point can be obtained from (1.1) as

$$\eta_{2c} \equiv \eta_1 \eta_3 \,. \tag{1.4}$$

This bifurcation is a Non-Smooth Fold (NSF), in which **F** and **S** co-exist if $\eta_2 > \eta_{2c}$ and neither exist if $\eta_2 < \eta_{2c}$. Note that the coalescence of a saddle **S** with a focus **F** can only occur because this is a non-smooth system. Such bifurcations do not arise in smooth systems where a SNB necessarily indicates collision of a stable node and a saddle. The mathematical structure near $(\eta_{2c}, 0)$ is substantially different from that near the smooth SNB $(\eta_{sf}, \mathcal{V}_{2sf})$, indicated by o in Figure 1. In particular at a NSF the real parts of the eigenvalues of the linearisations of either of the fixed points do not drop to zero.

In general, parameters are not static in climate models of this type, but rather can oscillate (seasonally for example) with a mean that can also drift over time. Variation of a parameter (typically η_2 in (1.1)) can lead to tipping, which in the context of this study corresponds to a solution starting at the focus **F** (or **N**) that does not stay close to **F** (or **N**) but rapidly evolves to a qualitatively different state, typically to **N** (or **F**) or to a large amplitude periodic orbit. Tipping often occurs when the variation drives a solution starting near **F** or **N** to encounter the unstable manifold of saddle **S**, or via a dynamic bifurcation through the underlying static fold point. Given the different characteristics of the fold points η_{2c} and η_{2sf}, we expect clear differences between the tipping near these different critical values. We note that tipping close to a NSF is different in many respects from tipping close to a SNB, because, as noted above, the eigenvalues of the linearisation of the system about the fixed point do not drop to zero in the non-smooth case.

To capture the impact of this parameter variation, we consider the case where both η_2 and η_1 oscillate rapidly, with the mean behavior of η_2 varying slowly in time. Specifically, we take

$$\eta_1 \to \eta_1 + B\sin(\Omega t) \quad \text{and} \quad \eta_2 \to \eta_2(t) + \hat{B}\sin(\Omega t)$$

in (1.1), where $\dot{\eta_2} = -\epsilon$ with $\epsilon \ll 1$ and $\Omega \gg 1$. We rewrite (1.1) in terms of the AMOC strength $\mathcal{V}$, which plays the role of the *switch parameter* (measuring the closeness of the solution to Σ), and set $A = B - \hat{B}$ to get

$$\begin{aligned} \dot{\mathcal{V}} &= \eta_1 - \eta_2(t) + \eta_3(\mathcal{T} - \mathcal{V}) - \mathcal{T} - \mathcal{V}|\mathcal{V}| + A\sin\Omega t, \\ \dot{\mathcal{T}} &= \eta_1 - \mathcal{T}(1 + |\mathcal{V}|) + B\sin\Omega t \\ \dot{\eta_2} &= -\epsilon, \qquad \epsilon \ll 1, \qquad \Omega \gg 1\,. \end{aligned} \tag{1.5}$$

As is typical for applied settings [5], we follow certain parameter assumptions; first, that $\eta_3 < 1$, which results in a SNB in (1.5) for the branch $\mathcal{V} > 0$. It is frequently assumed that the salinity's relaxation time is much longer than that of temperature, giving $\eta_3 < 1$. Furthermore, we take $\eta_1 = O(1)$ so that $\eta_{2c} = \eta_3\eta_1 = O(1)$ and $\eta_{2c} < \eta_{2sf}$. That is, there is a non-trivial bi-stability range for the two stable equilibria on the branches **N** ($\mathcal{V} > 0$) and **F** ($\mathcal{V} < 0$) as shown in Figure 1. For convenience of notation, we take A and B to be non-negative in our analysis below. The analysis for $A < 0$ or $B < 0$ is analogous, and yields the same identification of the tipping points in the case of high frequency forcing.

Our primary focus in this paper is on the tipping behavior as $\eta_2(t)$ in (1.5) varies dynamically close to the static NSF bifurcation point η_{2c}. Figure 1 illustrates this tipping behavior, where there is a relatively rapid transition between the salinity- and temperature-dominated states, **F** and **N**. From the results shown in Figure 1, without oscillatory forcing, the tipping via dynamic bifurcation is lagged relative to η_{2c}. In contrast, the tipping from **F** to **N** is advanced when there is oscillatory forcing, with increasing values of A/Ω increasing this advance. Below we explore the separate and combined effects of both slowly varying η_2 and a high frequency oscillatory forcing $\Omega \gg 1$ that drives tipping near the NSF point.

The influence of these types of variations have been explored in the context of a SNB [20], based on an analysis developed for its normal form, and employed in other applications. With a slowly varying bifurcation parameter $a(t)$, this normal form is

$$\dot{z}(t) = a(t) - z^2 + \mathcal{A}\sin(\Omega t), \quad a = a_0 - \epsilon t\,. \tag{1.6}$$

Combined multiple scales and local analyses yield analytical expressions for the location of the tipping point via dynamic bifurcation, relative to the static SNB at $a_c = 0$, $x_c = 0$. Results are qualitatively similar to those for the NSF shown in Figure 1, namely, the tipping is lagged for the dynamic bifurcation with no oscillations $\mathcal{A} = 0$, $\epsilon \neq 0$, advanced for oscillations only $\mathcal{A} \neq 0$, $\epsilon = 0$, and the lag and advance compete for the case with both slowly varying bifurcation parameter and oscillatory forcing.

Our goal in this paper is to develop a related multiple scale analytical approach for approximating the tipping point in the setting of a dynamic NSF bifurcation, including the case where there is also high frequency forcing. The analysis provides both precise quantitative and qualitative descriptions of the tipping behavior, from which we can determine the influence of dynamic parameters as well as of the oscillatory forcing. It might be expected, given that we are considering non-smooth systems, that it is necessary to construct piecewise-smooth solutions from which to obtain the tipping behavior [17]. However, for high frequency oscillatory forcing, we instead use a multiple

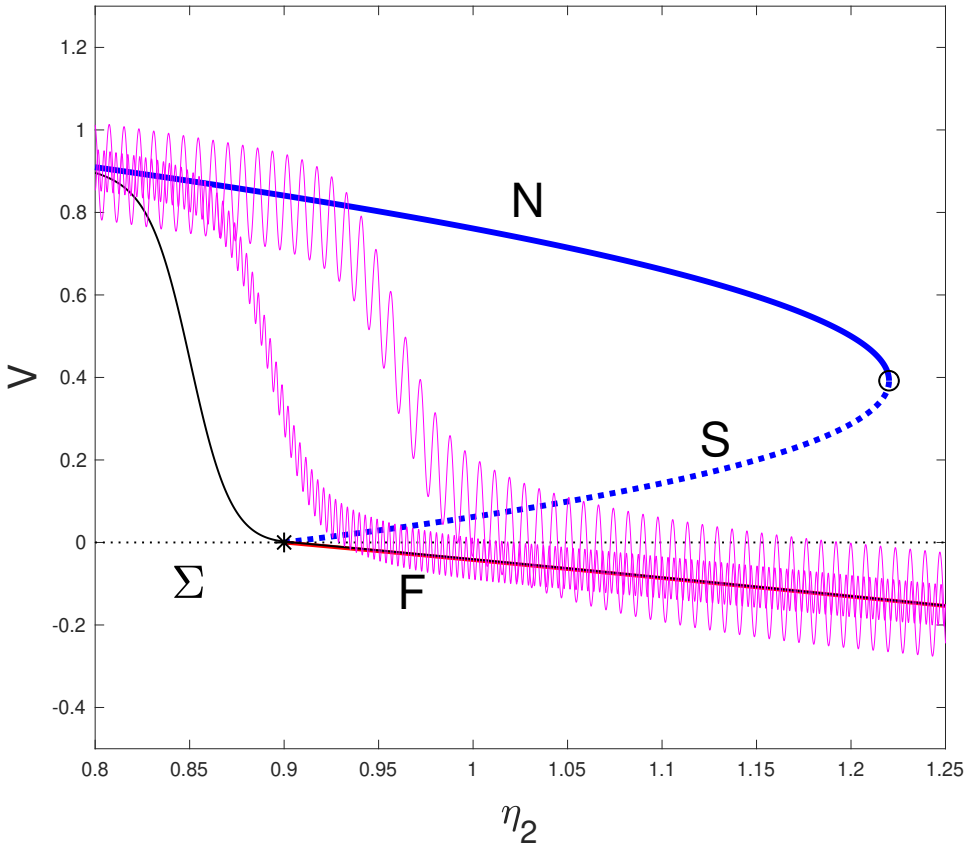

Figure 1: Tipping close to a NSF via dynamic bifurcation in (1.5) with both slowly varying and rapid oscillatory behavior of the parameter η_2 Blue and red curves give the equilibria for static parameters, solid lines indicate stable equilibria as a node (**N**) and focus (**F**), and the dotted line as a saddle (**S**). o indicates the smooth SNB at $(\eta_{2sf}, \mathcal{V}_{2sf})$, and $*$ indicates the NSF bifurcation at $(\eta_{2c}, 0)$. The black solid line corresponds to the solution of (1.5) with $\dot{\eta_2} = -\epsilon$ with no oscillatory forcing ($A = B = 0$). Magenta solutions correspond to both $\dot{\eta_2} = -\epsilon$ and A and B non-zero, with $\Omega \gg 1$, the ratio of $A/\Omega = 0.05$ (transition away from F closer to η_{2c}) and $A/\Omega = 0.125$. Here $\eta_1 = 3$, $\eta_3 = 0.3$, and $\epsilon = 0.05$.

scales approach in which we derive equations for the mean of the oscillatory solutions. When the oscillations cross the switching manifold Σ, they do not simply average out, but rather give nonlinear contributions to the dynamics of the mean behavior. From the nonlinear dynamics of the mean, we can then determine the shift in the tipping point relative to the static case. Furthermore, the approach provides information about the validity of the multiple scale approach based on the high frequency forcing oscillations. Then we have the range of frequencies over which the approximations are valid, relative to other parameters such the strength of the forcing and time scale of the dynamic bifurcation. These results also indicate the conditions under which a piecewise construction of the solution is needed to predict tipping, instead of capturing the averaged nonlinear effects of the non-smooth dynamics.

We develop this multi-scale approach first in the setting of a single degree-of-freedom (DoF) model with an underlying static bifurcation structure that mirrors certain aspects of the static Stommel Box model (1.5) close to the NSF. This is a relatively generic and simple model with a region of bi-stability of two stable states that lose stability via a smooth SNB or NSF bifurcation (in this case given by a coalescence of a saddle point and a node with the discontinuity surface Σ_x) for this single DoF system. The model provides a framework in which we can develop the asymptotic expressions for tipping points in three cases: slowly varying bifurcation parameter only, high frequency oscillatory forcing only, and both types of variation combined. We then extend the method to the case of the full two DoF Stommel Box model. The approach uses multiple scale approximations, based on the different time scales associated with the slow rate $\epsilon \ll 1$ of variation near or through the static bifurcation value, the period of the oscillations proportional to $\Omega^{-1} \ll 1$, and the time scale t of the model. The multiple scales analysis is applied to both outer and inner expansions, relevant away from and near the tipping point, respectively. Both the multiple time scales and the development of a local expansion are necessary to approximate the solution, leading to explicit expressions for the tipping points in different settings.

1.3 Paper Summary

The remainder of this paper is organized as follows. In Section 2 we consider the case of the dynamic bifurcation where the bifurcation parameter varies slowly through a static NSF in the single DoF problem and without oscillatory forcing. Section 3 covers the case where the bifurcation parameter is static and there is high frequency oscillatory forcing. It also discusses conditions under which the multiple scale analysis is appropriate to study tipping, in contrast to situations that would require a geometric-based approach that exploits the piecewise-smoooth structure of the problem [17] (postponed to future work). In Section 4 we consider the combined effects of slowly varying bifurcation parameter and high frequency oscillatory forcing. In each section we first demonstrate the approach on the single DoF model, constructing both outer and local expansions for the solutions from which we determine the tipping point or critical value of the bifurcation parameter. Then we use this same approach in the Stommel model to identify tipping points, the critical values of η_2 in each setting.

2 Dynamic bifurcation for a NSF

2.1 Overview

In this section we look at the problem of a dynamic bifurcation close to the non-smooth fold (NSF) in both the Stommel model and in the single DoF analogy to this model. We consider the case of a slowly changing bifurcation parameter without any oscillatory forcing. We show that in both cases the tipping close to the NSF is lagged relative to the location of the NSF. This behavior is

qualitatively similar to that found close to a saddle-node bifurcation (SNB). However the magnitude of the lag is different, as the eigenvalues of the fixed points do not drop to zero at the NSF, unlike the case of the SNB.

2.2 Dynamic bifurcation in the single degree-of-freedom model

In this subsection we use a single DoF non-smooth model to develop our approach and results for the dynamic bifurcation. In particular we consider the model:

$$\dot{x} = -\mu + 2|x| - x|x| + A\sin(\Omega t), \qquad \dot{\mu} = -\epsilon, \qquad x(0) = x^0, \quad \mu(0) = \mu^0 > 0,\ \epsilon \ll 1\,. \tag{2.1}$$

taking $A = 0$ in this case. As in the Stommel model, the presence of the $|x|$ term means that there is a discontinuity surface at $x = 0$, denoted by Σ_x. Across Σ_x the flow and its derivatives are continuous, but the second derivative of the flow is discontinuous.

As in the Stommel model, the underlying static model with $\epsilon = 0$ has two equilibrium branches, denoted $x^+_{\rm eq}$ and $x^-_{\rm eq}$ in Figure 2, with $x > 0$ and $x < 0$, respectively. The equilibrium $x^+_{\rm eq}$ loses stability via a SNB at $\mu_{\rm snb} = 1, x_{\rm snb} = 1$, so that it is stable for $x > 1$ and unstable for $0 < x < 1$. The discontinuity surface Σ_x yields a NSF bifurcation, where the equilibrium branch $x^-_{\rm eq}$ terminates at $\mu_c = 0, x_c = 0$, as shown in Figure 2. The NSF arises when the saddle and the node intersect with Σ_x. (This differs from the Stommel model in which we see an intersection of a saddle with a focus at the NSF). Observe that the corresponding eigenvalues of the linearisation at the NSF about the saddle and the node are ± 2 and hence do not vanish.

For slowly varying μ without oscillations ($A = 0$) we determine values of μ for which we have (non-smooth) tipping points (or dynamic bifurcations), at which the solution transitions from following $x^-_{\rm eq}$ to following $x^+_{\rm eq}$. We take initial conditions near the lower branch given by $x^0 = 1 - \sqrt{1+\mu^0} < 0$, and use a combination of outer and local asymptotic approximations for the solution x.

We first give an approximation for x for $O(1)$ slowly varying values of $\mu > 0$, that is, away from the NSF value of $\mu_c = 0$. Termed the outer expansion, it may appear that this approximation is not relevant to tipping, since it describes behavior away from $\mu_c = 0$ where the dynamics follow $x^-_{\rm eq}$ rather than experiencing tipping to another solution. However, this expansion provides the motivation for a valuable rescaling for μ near $\mu_c = 0$, on which an inner expansion is based. Approximating the solution with this inner expansion yields the calculation of the tipping point. To get the outer expansion, we look for a solution as a function of the slow time $\tau = \epsilon t$,

$$x(\tau) \sim x_0(\tau) + \epsilon x_1(\tau) + \epsilon^2 x_2(\tau) + O(\epsilon^3), \qquad \dot{x} = \epsilon \frac{dx}{d\tau} \equiv \epsilon x_\tau\,. \tag{2.2}$$

Substituting into (2.1) yields the sequence of equations at orders of ϵ^j,

$$O(1): \quad 0 = -\mu(t) - 2x_0 + x_0^2, \tag{2.3}$$

$$O(\epsilon): \quad x_{0\tau} = -2x_1 + 2x_1 x_0. \tag{2.4}$$

Note that as $x_0 < 0$ we take $|x| = -x$ in this approximation, yielding the asymptotic result for $\epsilon \ll 1$

$$x(t) \sim 1 - \sqrt{1+\mu(t)} - \frac{\epsilon}{4(1+\mu(t))} + O(\epsilon^2). \tag{2.5}$$

This solution is attracting for $x < 0$ and $\mu = O(1)$, as can be verified through a linear stability analysis, based on a multiple scale analysis. This approximation is no longer valid for values of

$\mu = O(\epsilon)$, since $x_0 = O(\epsilon)$ and the ordering of terms in (2.5) is no longer correct. Furthermore, for μ approaching 0, we must consider the possibility that x is not strictly negative, so that the non-smooth dynamics starts to play a role. Thus we use a local analysis near the critical value $(\mu_c, x_c) = (0, 0)$. We rescale x and μ near this value via

$$x = \epsilon\, y, \quad \mu = \epsilon\, m, \tag{2.6}$$

which we substitute into (2.1) to get the local equation,

$$\begin{aligned} \dot{y} &= -\, m(t) + 2|y| - \epsilon|y|^2, \\ \dot{m} &= -\, 1. \end{aligned} \tag{2.7}$$

From (2.1) we provide an approximation for y (and thus x) near the NSF at $\mu_c = 0$.

Since we are interested in the behavior of y as a function of m, we write the differentiation on y directly in terms of the parameter m. Taking $y \sim y_0 + \epsilon y_1$, we find the leading order equation for y_0,

$$\frac{dy_0}{dm} = m - 2|y_0|. \tag{2.8}$$

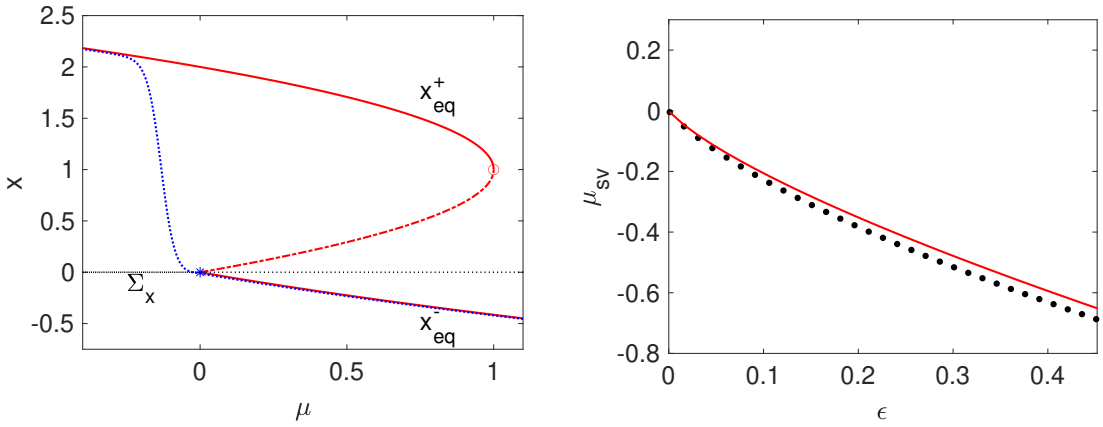

Figure 2: (Left) The bifurcation diagram for (2.1) with stable upper and lower equilibrium branches in red solid lines and the unstable middle branch shown with a red dash-dotted line. The NSF bifurcation occurs at (0,0) with the blue $*$ and the SNB occurs at (1,1) with the red o. The numerical solution (blue dotted line) to (2.1) is shown for $A = 0$ and $\epsilon = 0.05$. (Right) The tipping value for $\mu_{\rm sv}$ approximated by (2.11) (solid red line) and the numerical result from (2.1) (black dots) with $A = 0$, taking $x_{\rm tip} = 1$.

For $m > 0$, the leading order approximation for the attracting solution is $y_0 = -m/2 - 1/4$, which is the same as the leading order approximation to (2.5) written in terms of (2.6). From that result, we conclude that $y_0(-1/2) = 0$ and that $y_0 > 0$ for $m < -1/2$. Then we find the leading order approximation for the solution of (2.7) for $m < -1/2$,

$$y^+(m) = Ce^{-2m} + \frac{m}{2} - \frac{1}{4} + O(\epsilon) \quad \text{for} \quad m < -\tfrac{1}{2} \quad \text{and} \quad y > 0,$$

corresponding to the solution crossing Σ_x. Here C is chosen so that $y^+(-1/2) = 0$, for continuity of the solution across $y = 0$. In terms of the original variables, we then use (2.6) to provide the local approximation of x for $|\mu| \ll 1$,

$$\begin{aligned} &x(t) \sim -\tfrac{\mu}{2} - \tfrac{\epsilon}{4}, && \text{for } \mu > -\tfrac{\epsilon}{2} \\ &x(t) \sim \epsilon C e^{-2\mu(t)/\epsilon} + \tfrac{\mu(t)}{2} - \tfrac{\epsilon}{2} + o(\epsilon^2), && \text{for } \mu < -\tfrac{\epsilon}{2}, \qquad C = (2e)^{-1}\,. \end{aligned} \tag{2.9}$$

Note that this solution grows exponentially fast for $\mu < -\epsilon/2$, so that from (2.9) we identify the tipping value $\mu_{\rm sv}$ for which the solution x reaches $x = x_{\rm tip}$. A leading order approximation to $\mu_{\rm sv}$ in ϵ is given by

$$\mu^0_{\rm sv} \sim \frac{1}{2}\epsilon \log(\epsilon)\,, \tag{2.10}$$

and (2.10) can be used to obtain higher order corrections from (2.9),

$$\begin{aligned} \mu_{\rm sv} \sim \mu^0_{\rm sv} + \epsilon\mu^1_{\rm sv} + \epsilon^2 \frac{\log\epsilon + \mu^1_{\rm sv} - 1/2}{2x_{\rm tip}} \\ \mu^1_{\rm sv} = \frac{\log(C/x_{\rm tip})}{2}\,. \end{aligned} \tag{2.11}$$

In Figure 2 we compare (2.11) to the tipping value μ at which x reaches a critical value $x_{\rm tip} = 1$, obtained from simulations of the full system (2.1) with slowly varying μ and $A = 0$.

We contrast the result (2.11) with the tipping value for the dynamic bifurcation near a SNB as in (1.6) with $A = 0$, studied in [8]. There the the tipping value of $a = a_{\rm sv}$ is negative, so that the dynamic bifurcation is lagged relative to the static SNB value $a = 0$, with

$$0 > a_{sv} = O(\epsilon^{2/3}).$$

Note that this dependence of the tipping value on the slow rate ϵ is different from that of the dynamic NSF bifurcation given in (2.11). Then the dynamic bifurcations near an SNB and NSF are lagged relative to the corresponding static bifurcation points, but there is a longer lag for the SNB than for the NSF of (2.1). This is discussed further below, in the context of additional rapid oscillatory forcing (see Section 4.3).

2.3 Dynamic bifurcation in the Stommel model

We now turn our attention to (1.5), the transformed Stommel two-box model with slowly varying fresh water flux η_2,

$$\begin{aligned} \dot{\mathcal{V}} &= \eta_1 - \eta_2 + \eta_3(\mathcal{T} - \mathcal{V}) - \mathcal{T} - \mathcal{V}|\mathcal{V}| \\ \dot{\mathcal{T}} &= \eta_1 - \mathcal{T}(1 + |\mathcal{V}|) \\ \dot{\eta_2} &= -\epsilon \\ \mathcal{T}(0) = \mathcal{T}_i, &\quad \mathcal{V}(0) = \mathcal{V}_i, \quad \eta_2(0) = \eta_{2i} > \eta_1\eta_3\,. \end{aligned} \tag{2.12}$$

Here we have set $A = B = 0$ in (1.5), postponing the treatment of periodic forcing to later sections.

As in the analysis of (2.1), we seek an analytical expression for the tipping point $\eta_{2\rm sv}$ as η_2 varies through the NSF, $\eta_{2c} \equiv \eta_1\eta_3$. This tipping point corresponds to the rapid transition from solutions near the salinity-dominated branch of focus points **F** to the temperature-dominated branch of nodes **N** in Figure 1. We again first find the outer expansion, approximating the behavior away from η_{2c} where the dynamics follow **F** rather than experiencing tipping to another solution. This expansion again provides the motivation for a valuable rescaling for η_2 near η_{2c}, and for an inner expansion for the solution, from which we derive the tipping point.

With a focus on the lower branch **F** with $\mathcal{V} < 0$, we approximate the slowly varying outer solution $\mathcal{V}(\tau), \mathcal{T}(\tau)$, away from η_{2c}, by substituting in (2.12) a regular asymptotic expansion in ϵ,

$$\begin{aligned} \mathcal{V}(\tau) \sim &\mathcal{V}_0(\tau) + \epsilon\mathcal{V}_1(\tau) + \epsilon^2\mathcal{V}_2 + \dots \\ \mathcal{T}(\tau) \sim &\mathcal{T}_0(\tau) + \epsilon\mathcal{T}_1(\tau) + \epsilon^2\mathcal{T}_2(\tau) + \dots\,, \end{aligned} \tag{2.13}$$

using $\tau = \epsilon t$. For $\mathcal{V} < 0$ we obtain the sequence of equations as coefficients of powers of ϵ,

$$O(1): \quad \begin{cases} 0 = & \eta_1 - \eta_2(\tau) + \eta_3(\mathcal{T}_0 - \mathcal{V}_0) - \mathcal{T}_0 + \mathcal{V}_0^2, \\ 0 = & \eta_1 - \mathcal{T}_0(1 - \mathcal{V}_0), \end{cases} \tag{2.14}$$

$$O(\epsilon): \quad \begin{cases} \mathcal{V}_{0\tau} = & \eta_3(\mathcal{T}_1 - \mathcal{V}_1) - \mathcal{T}_1 + 2\mathcal{V}_1\mathcal{V}_0, \\ \mathcal{T}_{0\tau} = & -\mathcal{T}_1(1 - \mathcal{V}_0) + \mathcal{V}_1\mathcal{T}_0\,. \end{cases} \tag{2.15}$$

We solve (2.14) simultaneously for the pseudo-equilibria, treating $\eta_2(\tau)$ as a constant in the approximation,

$$\begin{aligned} \mathcal{T}_0(V_0) =& \frac{\eta_1}{1 - V_0}, \\ 0 = \eta_1 - \eta_2(\tau) - T_0(V_0) + \eta_3(T_0(V_0) - V_0) + V_0^2&. \end{aligned} \tag{2.16}$$

Corrections to the pseudo-equilibrium from (2.16) can be obtained from (2.15), which are used below in the detailed calculation of the tipping point.

The expansion (2.13) breaks down if $\mathcal{V}$ approaches zero, and we note this is the case in the vicinity of the NSF, $(\mathcal{T}, \mathcal{V}, \eta_{2c}) = (\eta_1, 0, \eta_1\eta_3)$. We perform a separate local analysis analogous to Section 2.2 using a similar scaling, at $\eta_{2c} = \eta_1\eta_3$. Specifically, we substitute

$$\eta_2 = \eta_1\eta_3 + \epsilon\zeta, \qquad \mathcal{V} = \epsilon X, \qquad \mathcal{T} = \eta_1 + \epsilon Y. \tag{2.17}$$

into (2.12) to get

$$\begin{aligned} \dot{X} &= -\zeta(t) - \eta_3 X - (1 - \eta_3)Y - \epsilon X|X|, \\ \dot{Y} &= -\eta_1|X| - Y - \epsilon|X|Y, \qquad \dot{\zeta} = -1. \end{aligned} \tag{2.18}$$

By linearizing (2.18) for $X \ll 1$ and $Y \ll 1$, specifically,

$$\begin{pmatrix} \dot{X} \\ \dot{Y} \end{pmatrix} = \begin{pmatrix} -\eta_3 & -(1 - \eta_3) \\ -\eta_1 \mathrm{sgn}(X) & -1 \end{pmatrix} \begin{pmatrix} X \\ Y \end{pmatrix} - \begin{pmatrix} \zeta(t) \\ 0 \end{pmatrix}, \tag{2.19}$$

we can approximate the location of the tipping point for solutions transitioning from **F** to **N**.

For $\zeta > 0$ and $X < 0$ ($\mathcal{V} < 0$) the eigenvalues in (2.19) have negative real part for $\eta_3 < 1$ and $\eta_1 > 1$ such that $\eta_3\eta_1 = O(1)$, as discussed following (1.4). Then we do not see growth of the solution away from **F**. As ζ decreases, eventually we have $\mathcal{V} > 0$ and the dynamics changes. Using $\dot{\zeta} = -1$ together with the chain rule $\frac{d}{dt} = \frac{d}{d\zeta}\frac{d\zeta}{dt}$ to replace $\frac{d}{dt}$ with $-\frac{d}{d\zeta}$ in (2.19) we solve

$$\begin{pmatrix} X_\zeta \\ Y_\zeta \end{pmatrix} = \mathbf{M} \begin{pmatrix} X \\ Y \end{pmatrix} + \begin{pmatrix} \zeta \\ 0 \end{pmatrix}, \qquad \mathbf{M} = \begin{pmatrix} \eta_3 & 1 - \eta_3 \\ \eta_1 & 1 \end{pmatrix}. \tag{2.20}$$

The solution is based on the corresponding eigenvalues

$$\lambda_{1,2} = \frac{\eta_3 + 1}{2} \pm \frac{1}{2}\sqrt{(1 + \eta_3)^2 + 4(\eta_1(1 - \eta_3) - \eta_3)}\,, \tag{2.21}$$

which are real, since $\eta_3 < 1$ guarantees that the discriminant is always positive. However, since we have one positive and one negative eigenvalue, $\lambda_1 < 0 < \lambda_2$, we have exponential growth for $X > 0$, which takes the form for $\mathbf{X} = (X, Y)^\top$,

$$\mathbf{X}(\zeta) \sim \mathbf{K}_1 e^{\lambda_1\zeta} + \mathbf{K}_2 e^{\lambda_2\zeta} + \mathbf{C}_1\zeta + \mathbf{C}_2\,. \tag{2.22}$$

Here $\mathbf{C}_1$ $\mathbf{C}_2$ are obtained from the particular solution of (2.20), namely, $\mathbf{C}_1 = \mathbf{M}\mathbf{C}_2$, $\mathbf{M}\mathbf{C}_1 = -(1\ 0)^\top$. Writing (2.22) in terms of the original variables $\mathcal{V} = \epsilon X$ and $\eta_2 = \eta_{2c} + \epsilon\zeta$, we find the approximation

$$\begin{aligned} \mathcal{V}(t) \ &\sim C_{11}(\eta_2(t) - \eta_{2c}) + \epsilon C_{12} + \epsilon K_{11} e^{\lambda_1(\eta_2(t)-\eta_{2c})/\epsilon} + O(\epsilon^2)\,. \\ \mathbf{C}_j &= (C_{j1}\ C_{j2})^\top \qquad \mathbf{K}_j = (K_{j1}\ K_{j2})^\top \end{aligned} \tag{2.23}$$

Note that we drop the term with coefficient $\mathbf{K}_2$ since $\lambda_2 > 0$ and that term is exponentially small for $\zeta < 0$.

Approximating K_{11} as described in Appendix A.1, using (2.16) and the expressions for $\mathbf{C}_j$, completes the approximation of $\mathcal{V}$ in (2.23). Taking logarithms in (2.23) yields an equation for the tipping value $\eta_{2\mathrm{sv}}$, at which $\mathcal{V}$ reaches $\mathcal{V}_{\mathrm{tip}}$,

$$\eta_{2\mathrm{sv}} \sim \eta_{2c} - \frac{\epsilon}{\lambda_1}\left[\log\epsilon - \log(\mathcal{V}_{\mathrm{tip}}) + \log\ K_{11}\right] - \frac{e^{-\lambda_1(\eta_{2\mathrm{sv}}-\eta_{2c})/\epsilon}}{K_{11}\lambda_1}(C_{11}(\eta_{2\mathrm{sv}} - \eta_{2c}) + \epsilon C_{12})\,. \tag{2.24}$$

Similar to μ_{sv} in (2.10)-(2.11), we obtain the leading order contribution to $\eta_{2\mathrm{sv}}$ which is then in turn used to compute higher order corrections,

$$\begin{aligned} \eta_{2\mathrm{sv}} \ &\sim \ \eta^0_{2\mathrm{sv}} + \eta^1_{2\mathrm{sv}} + \frac{\epsilon^2}{2V_{\mathrm{tip}}}\left[\frac{C_{11}}{\lambda_1}\log\epsilon - C_{11}\eta^1_{2\mathrm{sv}} + \epsilon C_{12}\right] \\ \eta^0_{2\mathrm{sv}} \ &= \ \eta_{2c} - \frac{\epsilon}{\lambda_1}\log\epsilon \qquad \eta^1_{2\mathrm{sv}} = \frac{\epsilon}{\lambda_1}\left[-\log(\mathcal{V}_{\mathrm{tip}}) + \log(K_{11})\right]. \end{aligned} \tag{2.25}$$

The expression for $\eta_{2_{\mathrm{sv}}}$ results in a lag in the tipping of $O(\epsilon \ln \epsilon)$ relative to the NSF bifurcation η_{2c}. It is noticeably similar to the leading order term for μ_{sv} from Section 2.2. In Figure 3 we compare the analytical approximation for $\eta_{2_{\mathrm{sv}}}$ to numerical results.

3 High frequency oscillatory forcing

3.1 Overview

In this section we look at the influence of high frequency oscillatory forcing on the attracting solutions in both the Stommel model and in the single DoF analogous model (2.1) close to the NSF. In both cases we restrict our attention to a constant bifurcation parameter, that can be viewed as the mean of the forcing. We determine the critical value of the bifurcation parameter at which tipping is observed, with the attracting solution shifting from the lower branch (x^-_{eq} in (2.1) and $\mathbf{F}$ in the Stommel model) to the upper branch (x^+_{eq} in (2.1) and $\mathbf{N}$ in the Stommel model). In both cases the critical value of the bifurcation parameter is greater than the value of the static NSF, corresponding to an advance of the critical parameter. While in general one might expect in the non-smooth setting to have to construct a piecewise-smooth-type solution as the basis for a stability analysis [17], in the case of high frequency forcing we develop a multiple scale, averaging-type approach that captures the contribution of the oscillations to the shift in the critical parameter value.

3.2 The single DoF model

We first analyze the influence of oscillatory (seasonal) forcing near the NSF bifurcation in the single DoF model (2.1) for constant $\mu > 0$. That is, we take $A \sim O(1)$, $\Omega \gg 1$ and $\epsilon = 0$. As for the Stommel model, we take $A > 0$ for convenience of notation, noting that the same results for tipping are obtained for $A < 0$. For high frequency forcing, $\Omega \gg 1$, we have both an $O(1)$ time scale t

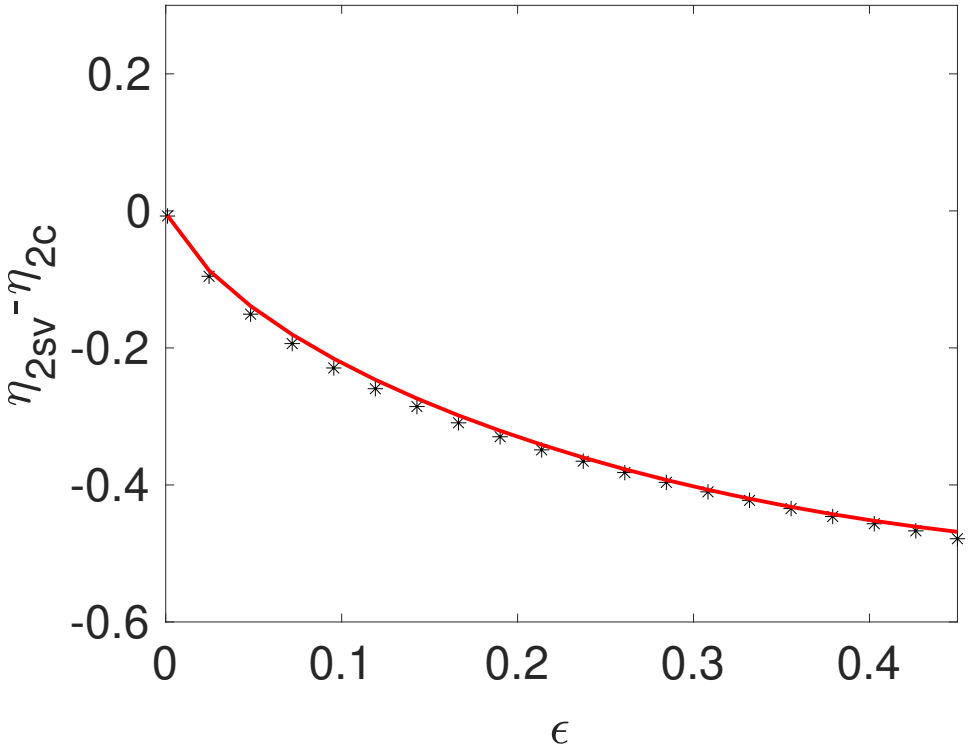

Figure 3: The tipping value for $\eta_2 - \eta_{2c}$ approximated by (2.24) (solid red line) compared to the numerical result from (2.12) (black stars) with $A = 0$, taking $\mathcal{V}_{\text{tip}} = .5$, $\eta_1 = 4$ and $\eta_3 = \frac{3}{8}$.

for the overall evolution and a fast time scale $T = \Omega t$ for the forcing. We use a multiple scales approximation $x(t) = x(t, T)$ to give an asymptotic approximation for the attracting solution near x_{eq}^-. We note that for large Ω the response of the solution to the forcing is $\mathcal{O}(1/\Omega)$ in magnitude, and this guides our overall analysis. From the behavior of this approximation, we obtain the critical value of μ below which there is no longer an attracting solution near x_{eq}^- [16].

First we determine the outer solution for which $x(t) < 0$. A simple ansatz of the form $x(t) = \overline{x} + R\cos(\Omega t)$ yields the structure of the attracting periodic behavior for large t,

$$x \sim 1 - \sqrt{1+\mu} - \Omega^{-1} A\cos(\Omega t) + O(\Omega^{-2}). \tag{3.1}$$

The form of (3.1) is motivated via a linear analysis or via a multiple scales analysis. The details of determining (3.1) via a formal multiple scales expansion are outlined in Appendix A.2.1. While this approach is not needed to obtain this simple outer solution, the steps provide a useful template, valuable for more complex cases in the sections below, for both outer solutions and local solutions from which the tipping values are determined.

Since the result is obtained only for the region for which $x < 0$, the solution in the form (3.1) is valid only when $A/\Omega < |1 - \sqrt{1+\mu}|$. If μ is small this region is approximated by taking the range $A/\Omega < \mu/2$.

For $\Omega \gg 1$, we now look for an inner solution for $\mu \ll 1$, specifically for

$$0 < \mu \leq \frac{2A}{\Omega}. \tag{3.2}$$

Thus we consider the solution as μ approaches $\mu_c = 0$, with $x(t)$ then taking both positive and negative values and hence with the non-smooth effects being important. We rescale x and μ via a

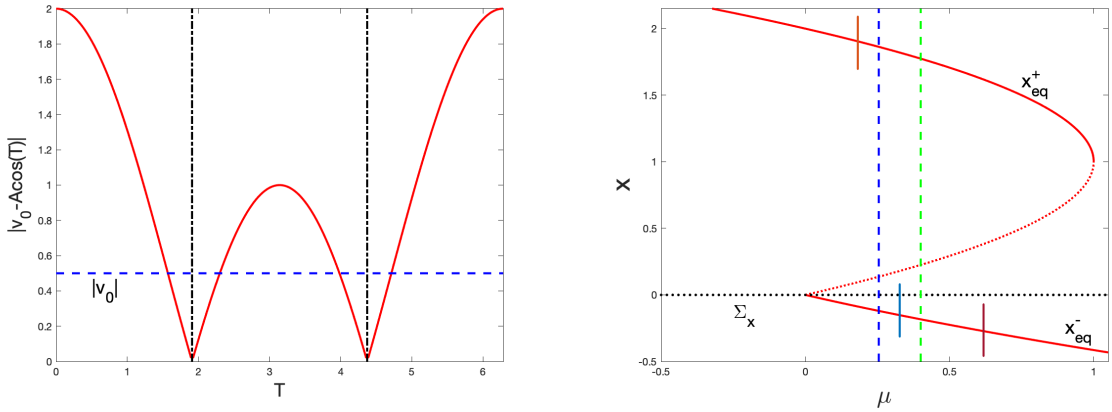

Figure 4: (Left)The non-smooth function $|v_0 - A\cos(T)|$ is shown by the solid red line, with dash-dotted vertical black lines indicating T_1 and T_2 from (3.8) for a sample value of v_0 shown by the dotted blue line. (Right) Attracting solutions of (2.1) for $\epsilon = 0$, $A = 2$ and $\Omega = 10$ are shown by short vertical lines superimposed on the static bifurcation diagram for x. The dashed vertical green line indicates $\mu = 2A/\Omega$, with (3.1) valid for $\mu > 2A/\Omega$. The dashed vertical blue line indicates the critical value $\mu_{\rm osc}$ (3.10). Note that for values between these two dashed lines, the attracting solution for x takes both positive and negative values. For $\mu < \mu_{\rm osc}$, the attracting solution is centered near $x^+_{\rm eq}$.

straightforward balancing argument,

$$m = \Omega^{-1}\mu, \qquad x = \Omega^{-1}y\,, \tag{3.3}$$

and introduce a multiple scales expansion for the local variable y,

$$y(t,T) \sim y_0(t,T) + \Omega^{-1}y_1(t,T) + O(\Omega^{-2}). \tag{3.4}$$

Substituting this expansion into (2.1) yields

$$O(1): \quad y_{0T} = A\sin(T), \tag{3.5}$$

$$O(\Omega^{-1}): \quad y_{1T} + y_{0t} = -m + 2|y_0|. \tag{3.6}$$

Solving the leading order equation (3.5) yields $y_0(t,T) = v_0(t) - A\cos(T)$ for an unknown function $v_0(t)$. Then applying the solvability condition (A.5) to (3.6) leads to

$$v_{0t}(t) = -m + \frac{1}{\pi}\int_0^{2\pi} |v_0(t) - A\cos(T)|\, dT. \tag{3.7}$$

The case where $A < |v_0|$ for all t yields $v_0 \approx -m/2$, corresponding to the expression (3.1) for $\mu \ll 1$ and $x < 0$ for all t. Therefore we restrict our attention to the case where $A > |v_0|$ and $\mu > 0$, corresponding to the solution x that crosses the discontinuity boundary Σ_x. In order to evaluate the integral in (3.7), we break the integration into regions based on the sign of $v_0 - A\cos(T)$, noting that the zeros of the integrand occur at

$$T = T_1 = \arccos(v_0/A), \qquad T = T_2 = 2\pi - \arccos(v_0/A), \qquad 0 < T_1 < T_2 < 2\pi\,, \tag{3.8}$$

as shown in Figure 4. Treating $v_0(t)$ as a constant relative to T under the multiple scales approxi-

mation, we evaluate the integral in (3.7) and use $\sin(\arccos(x)) = \sqrt{1-x^2}$ to get the equation for v_0,

$$v_{0t} = -m + \frac{4}{\pi}\left(\arcsin(v_0/A)v_0 + \sqrt{A^2 - v_0^2}\right) = \mathcal{F}(v_0; m)\,. \tag{3.9}$$

We find the critical value of m below which there is no stable equilibrium solution to (3.9) for v_0. The function $\mathcal{F}(v_0; m)$ (3.9) has a minimum with respect to v_0 at $v_0 = 0$. For values of m above the critical value $m = m_{\rm osc}$, $\mathcal{F}(v_0^*; m) = 0$ at the stable equilibrium $v_0^* < 0$ of (3.9). At the critical value of $m = m_{\rm osc}$, $\mathcal{F}(0; m_{\rm osc}) = 0$. Thus, we find that there is no attracting solution for v_0 for $m < m_{\rm osc} = 4A/\pi$. Written in terms of μ, $m_{\rm osc}$ is then

$$\mu_{\rm osc} \equiv \frac{4A}{\pi\Omega}. \tag{3.10}$$

From (3.9) we can obtain the equilibrium for v_0 implicitly for $\mu > \mu_{\rm osc}$. A Taylor expansion about the critical value, for $v_0/A = 0$, yields the approximate equation

$$v_{0t} \approx -m + \frac{4A}{\pi} + \frac{2}{\pi A}v_0^2, \tag{3.11}$$

which gives an explicit expression approximating the equilibrium solution

$$v_0 \approx -\sqrt{\frac{\pi A}{2}\left(m - \frac{4A}{\pi}\right)}. \tag{3.12}$$

Then, the approximate attracting solution to (2.1) for $\mu > \mu_{\rm osc}$, in terms of x and μ is

$$x(t) \sim -\sqrt{\Omega^{-1}\left(\mu - \frac{4|A|}{\pi\Omega}\right)} - \Omega^{-1}A\cos(\Omega t) + O(\Omega^{-2}). \tag{3.13}$$

For $\mu < \mu_{osc}$, there is no attracting solution near the lower bifurcation branch $x_{\rm eq}^-$, but instead $|v_0|$ increases rapidly, moving away from $x_{\rm eq}^-$, due to contributions from the absolute value nonlinearity in (3.7). This is shown in Figure 5, where the attracting solution for $\mu < \mu_{\rm osc}$ obtained computationally is shown centered around the upper bifurcation branch $x_{\rm eq}^+$, while for $\mu > \mu_{\rm osc}$ the attracting solution x remains near $x_{\rm eq}^-$. Since $\mu_{\rm osc} > 0$ for $A \neq 0$, the oscillations advance this critical value relative to $\mu_c = 0$ from the static, unforced case ($A = 0$). Then the range of μ for which there is bi-stability of $x_{\rm eq}^-$ and $x_{\rm eq}^+$ is reduced with oscillatory forcing, implying that this bi-stable region can be eliminated entirely for certain A and Ω.

In Figure 5 we compare the critical values of $\mu = \mu_{\rm osc}$ with the critical values observed from simulations of (2.1) for different values of A and Ω, indicating good agreement for a range of A/Ω. As expected, for larger values of Ω the approximation improves. For smaller values of Ω or larger values of A, the approximation is less accurate: in those cases x is dominated by oscillations that approach both $x_{\rm eq}^-$ and $x_{\rm eq}^+$, which violates both the assumption that the expansion (3.4) is near $x_{\rm eq}^-$ and the separation of scales assumption used to evaluate (3.7), on which (3.10) is based.

3.3 The Stommel model

We now consider the full Stommel system with oscillatory forcing given by (1.5) with $A, B \sim O(1)$, $\Omega \gg 1$ and $\epsilon = 0$. Similar to the analysis given in Section 3.2, we expect to find an attracting oscillatory solution centered near **F** in Figure 1 for parameter values $\eta_2 > \eta_{2\rm osc}$, where $\eta_{2\rm osc}$ is the critical value below which such an attractor no longer exists.

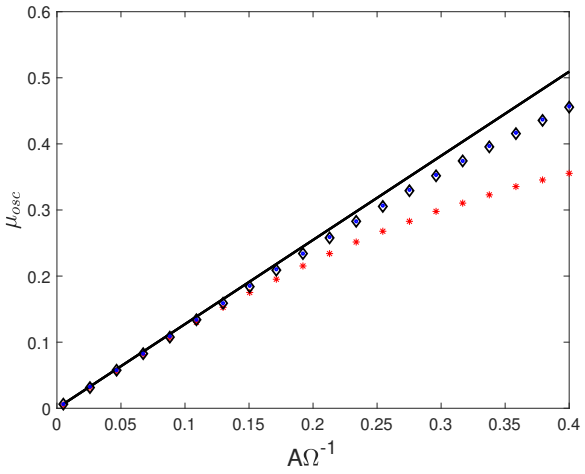

Figure 5: The critical value $\mu_{\rm osc}$ obtained from (3.10) (black solid line) compared with the numerically obtained values of $\mu_{\rm osc}$, based on the attracting behavior for large t of x from simulations of (2.1) with $\epsilon = 0$. For $\mu < \mu_{\rm osc}$ computational solutions of (2.1) do not remain centered near $x_{\rm eq}^-$ for large t. Results are shown for different amplitudes: $A = .5$ (red $*$'s), $A = 4$ (black diamonds), and $A = 8$ (blue o's).

We again take $\Omega \gg 1$, so that there are again slow t and fast $T = \Omega t$ time scales. Again the response to the forcing is small, of $\mathcal{O}(A/\Omega, B/\Omega)$, so that the forced dynamics can be well approximated by the linearisation of the Stommel model around its fixed points if Ω is large, and/or if A, B are small (a case to be considered in a later paper). Then substituting the appropriate multiple scale expansions in Ω^{-1} for $\mathcal{V} = \mathcal{V}(t, T)$ and $\mathcal{T} = \mathcal{T}(t, T)$, as shown in Appendix A.2.2, we obtain the approximate outer solution corresponding to oscillations of amplitude $A\Omega^{-1}$ centered on the salinity-dominated branch $\mathbf{F}$ of the form,

$$\begin{aligned} \mathcal{V} \sim& \mathcal{V}_0 - \Omega^{-1} A\cos(T) + \Omega^{-1}\mathcal{V}_{11}(t)\ldots \\ \mathcal{T} \sim& \mathcal{T}_0 - \Omega^{-1} B\cos(T) + \Omega^{-1}\mathcal{T}_{11}(t)\ldots \end{aligned} \tag{3.14}$$

where $\mathcal{V}_0$ and $\mathcal{T}_0$ are the equilibrium values on $\mathbf{F}$ and $\mathcal{V}_{11}$ and $\mathcal{T}_{11}$ give corrections on the t time scale to the oscillatory terms $A\sin(T)$ and $B\sin(T)$. We do not have explicit expressions for these corrections, but a local stability analysis shows that these terms remain small for $O(1)$ values of $\eta_2 - \eta_{2c} > 0$.

Significantly, this approximation breaks down when, for example, $\mathcal{V}_0 \sim A\Omega^{-1}$ and the solution may then intersect Σ. Since $\mathcal{V}_0$ decreases linearly with $\eta_2 - \eta_{2c} > 0$, and as $A = \mathcal{O}(1)$, then similarly to the behavior of the single DoF model above in Section 3.2, this approximation breaks down for parameter values near the NSF value, that is, for $\eta_2 - \eta_{2c} = O(\Omega^{-1})$. To consider these values, we rescale

$$\mathcal{V} = \Omega^{-1} X, \qquad \mathcal{T} = \eta_1 + \Omega^{-1} Y, \qquad \eta_2 = \eta_1\eta_3 + \Omega^{-1}\zeta. \tag{3.15}$$

Substituting (3.15) into (1.5), together with the multiple scales expansion,

$$\begin{aligned} X(t, T) \sim& X_0(t, T) + \Omega^{-1} X_1(t, T) + O(\Omega^{-2}), \\ Y(t, T) \sim& Y_0(t, T) + \Omega^{-1} Y_1(t, T) + O(\Omega^{-2}), \end{aligned} \tag{3.16}$$

yields the series at sequential powers of Ω^{-1}. We then have the inner system of equations for X

and Y near η_{2c} ($\zeta = 0$),

$$O(1): \quad \begin{cases} X_{0T} = & A\sin(T), \\ Y_{0T} = & B\sin(T), \end{cases} \tag{3.17}$$

$$O(\Omega^{-1}): \quad \begin{cases} X_{1T} + X_{0t} = & -\zeta - \eta_3 X_0 - (1-\eta_3)Y_0, \\ Y_{1T} + Y_{0t} = & -\eta_1|X_0| - Y_0\,. \end{cases} \tag{3.18}$$

From (3.17) we find that the leading order terms are

$$X_0 = P_0(t) - A\cos(T), \quad Y_0 = Q_0(t) - B\cos(T)\,. \tag{3.19}$$

for P_0, Q_0 functions of the slow time scale t, which must be determined in order to locate the center of the oscillations. Substituting (3.19) into (3.18), we apply the solvability condition (A.5) to get the equations for P_0 and Q_0

$$\begin{aligned} P_{0t} =& -\zeta - \eta_3 P_0 - (1-\eta_3)Q_0, \\ Q_{0t} =& -\frac{\eta_1}{2\pi}\int_0^{2\pi} |P_0 - A\cos(T)|dT - Q_0\,. \end{aligned} \tag{3.20}$$

The case $A < |P_0|$ corresponds to $\mathcal{V} < 0$, which is treated in the outer expansion above. For the range of η_2 where $|P_0(t)| < A$, the integral in (3.20) has the same form as in (3.7). We use the same approach to evaluate it as described in (3.7)-(3.8), replacing v_0 with P_0, and treating P_0 as a constant relative to integration over the fast time T. Similar to Section 3.2, the argument of the absolute value alternates sign over the regions delineated by T_1 and T_2, where $T_1 = \arccos(P_0/A)$ and $T_2 = 2\pi - \arccos(P_0/A)$. Integrating over each region to evaluate (3.20) yields

$$P_{0t} = -\zeta - \eta_3 P_0(t) - (1-\eta_3)Q_0, \tag{3.21}$$

$$Q_{0t} = -\frac{2\eta_1}{\pi}\left(\arcsin(P_0/A)P_0 + \sqrt{A^2 - P_0^2}\right) - Q_0\,. \tag{3.22}$$

In the high frequency forcing case of $\Omega \gg 1$, we use a quasi-steady approximation, discussed further in Section 3.4. We set $Q_{0t} = 0$ in (3.22), solve for Q_0 and substitute in (3.21), yielding

$$P_{0t} = -\zeta - \eta_3 P_0(t) - (1-\eta_3)\frac{2\eta_1}{\pi}\left(\arcsin(P_0/A)P_0 + \sqrt{A^2 - P_0^2}\right) \equiv \mathcal{G}(P_0;\zeta)\,. \tag{3.23}$$

As in Section 3.2, we find the critical value of ζ by looking for the maximum value of ζ for which there is no equilibrium solution for P_0 in (3.23). The function $\mathcal{G}(P_0;\zeta)$ in (3.9) has a minimum at $P_{0\min} = A\sin\left(\eta_3\pi/[2(1-\eta_3)\eta_1]\right)$. For $\mathcal{G}(P_{0\min};\zeta) < 0$, the value $P_0 < P_{0\min}$ at which $\mathcal{G}(P_0;\zeta) = 0$ corresponds to the stable equilibrium of (3.23). At the critical value of $\zeta = \zeta_{\rm osc}$, $\mathcal{G}(P_{0\min};\zeta_{\rm osc}) = 0$. Thus, we find that there is no attracting solution for P_0 in (3.23) for $\zeta < \zeta_{\rm osc}$, where

$$\zeta_{\rm osc} = \frac{2(1-\eta_3)\eta_1}{\pi}A\cos\left(\frac{\eta_3\pi}{2(1-\eta_3)\eta_1}\right) \implies \eta_{2_{\rm osc}} = \eta_1\eta_3 + \Omega^{-1}\zeta_{\rm osc}. \tag{3.24}$$

Then $\eta_{2_{\rm osc}}$ corresponds to the critical value of η_2, below which the attracting high frequency oscillatory solution of (1.5) with $\epsilon = 0$ does not remain near the salinity-dominated branch **F** in Figure 1. Note that the expression (3.24) indicates an advance of the critical value relative to $\eta_{2c} = \eta_1\eta_3$, for the restriction on $\eta_3 < 1$ discussed in Section 1.

In Figure 6 we compare (3.24) to the results observed from numerical simulations of (1.5) over a range of Ω^{-1}. We note that the approximation (3.24) breaks down for larger values of A/Ω. We discuss the source of this breakdown in Section 3.4, which has implications for the case where $\epsilon \neq 0$, and for cases with lower frequency forcing.

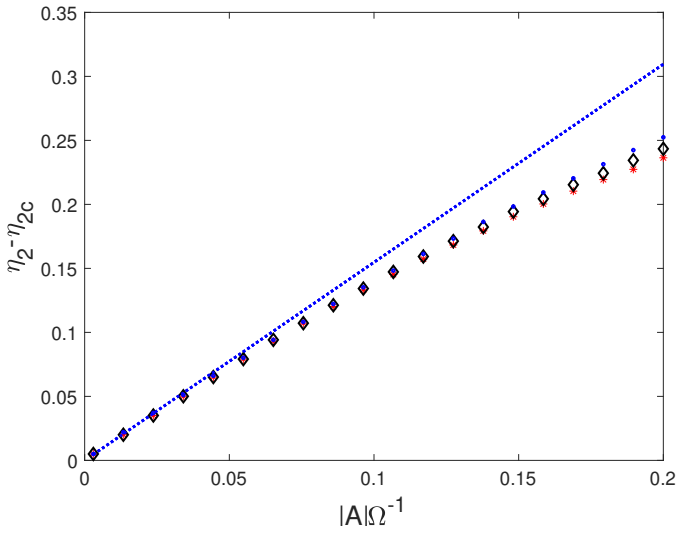

Figure 6: The critical value $\eta_{2_{\rm osc}}$ from (3.24) (blue dotted lines) compared with the critical value obtained from simulations of (1.5) with $\eta_1 = 4$, $\eta_3 = \frac{3}{8}$, and $\epsilon = 0$. The values for the forcing are $A = -1$, $B = 0$: red $*$'s; $A = 1$, $B = 2$: black diamonds; $A = 4$, $B = 5$: blue $\cdot$'s.

3.4 Linear analysis of the Stommel model near to the NSF

In Figure 7 we graph the attracting solution $\mathcal{V}$ and $\mathcal{T}$ of (1.5) in the $\mathcal{V} - \mathcal{T}$ plane, for $\epsilon = 0$ and for values of η_2 for which the solution stays near the salinity-dominated branch **F**. These are superimposed on the static bifurcation branches, **F** and **S** in the $\mathcal{V} - \mathcal{T}$ plane. We compare the result obtained from the multiple scale, averaging-type approximation (3.19) for high frequency forcing to that obtained from the simulation of (1.5). For example, for the forcing $A\sin(T)$ and $B\sin(T)$ in (1.5),

$$\mathcal{V} \sim \Omega^{-1}[P_0 - A\cos(\Omega t)] \qquad \mathcal{T} \sim \eta_1 + \Omega^{-1}[Q_0 - B\cos(\Omega t)]\,. \tag{3.25}$$

We show the results for different types of oscillatory forcing. These results illustrate good agreement for these solutions for larger Ω, supporting the good approximation of the critical value $\eta_{2_{\rm osc}}$, as shown in Figure 6. Comparisons of the solutions for smaller Ω (larger $A\Omega^{-1}$) also illustrate the source of the over-estimation of $\eta_{2_{\rm osc}}$ in these cases.

The main observation is that for larger frequency Ω (upper row in Figure 7), the multiple scale approximation (3.25) is accurate, even for solutions that cross both Σ and **S** when $\eta_2 \lesssim \eta_{2_{\rm osc}}$. Thus $\eta_{2_{\rm osc}}$ yields a good approximation for the critical value. Specifically, this approximation uses a construction composed of an oscillatory term, and the mean of these oscillations given by $(P_0/\Omega, \eta_1 + Q_0/\Omega)$ in (3.22) as a function of η_2. Nonlinear contributions from the integral in (3.20), when the oscillations in $\mathcal{V}$ cross the switching manifold Σ, shift this mean away from the equilibrium branch **F**. In Section 3.3 we obtained an explicit expression for the tipping point $\eta_{2_{\rm osc}}$ by using a quasi-stationary approximation for $(\mathcal{P}_0/\Omega, \mathcal{Q}_0/\Omega)$. A linear stability analysis of (3.22) indicates the basis for this approximation, namely, that a change in the linear stability of $(\mathcal{P}_0, \mathcal{Q}_0)$ occurs for $\mathcal{P}_0$ above a critical value,

$$\mathcal{P}_0 \sim \frac{A\pi\eta_3}{2\eta_1(1-\eta 3)}\,. \tag{3.26}$$

Figure 8 shows that $\mathcal{P}_0$ terminates in the black horizontal dotted lines corresponding to (3.26). As is consistent with simulations, as η_2 reaches its critical value, $\mathcal{P}_0$ reaches (3.26), while $\mathcal{Q}_0$ remains negative. Thus the tipping is primarily driven by variations in $\mathcal{V}$, captured in the dynamics of $\mathcal{P}_0$.

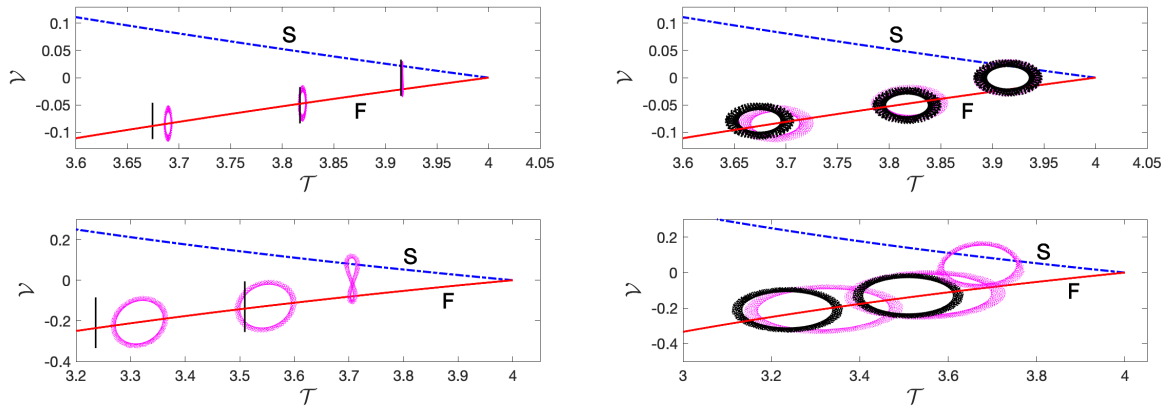

Figure 7: Comparison of the attracting (large t) oscillating solutions $\mathcal{V}$ and $\mathcal{T}$ in the $\mathcal{V}-\mathcal{T}$ phase plane for three different values of η_2, with $\eta_1 = 4$ and $\eta_3 = 3/8$. For each solution, $\eta_2 > \eta_{2\text{num}}$, where $\eta_{2\text{num}}$ is the critical value of η_2 obtained from the numerical solutions, as shown by the markers in Figure 6. The solution is closer to the NSF at $\mathcal{V} = 0$ and $\mathcal{T} = \eta_1$ for smaller η_2. The graphs obtained from the multiple scale approximation (3.25) (black) and numerical solutions (magenta) are super-imposed on the branches for the static equilibria **F** (red solid) and **S** (blue dash-dotted). Upper: For smaller values of A/Ω ($|A|/\Omega = 0.033$), (3.25) is in agreement with the numerical simulations. Lower: For larger values of A/Ω, ($|A|/\Omega = 0.125$) (3.25) does not fully capture the behavior of $\mathcal{V}$ and $\mathcal{T}$. Specifically, for $\eta_{\text{num}} < \eta_2 < \eta_{2\text{osc}}$, (3.25) over-estimates the advance of the tipping and there is no asymptotic approximation from (3.25) shown. Left: The forcing is $A\sin(T)$, $B = 0$. Right: $A = -1, B = 1$, with the forcing given by $A\sin(T)$ and $B\cos(T)$ (in contrast with $A\sin(T)$ and $B\sin(T)$ as in (1.5)).

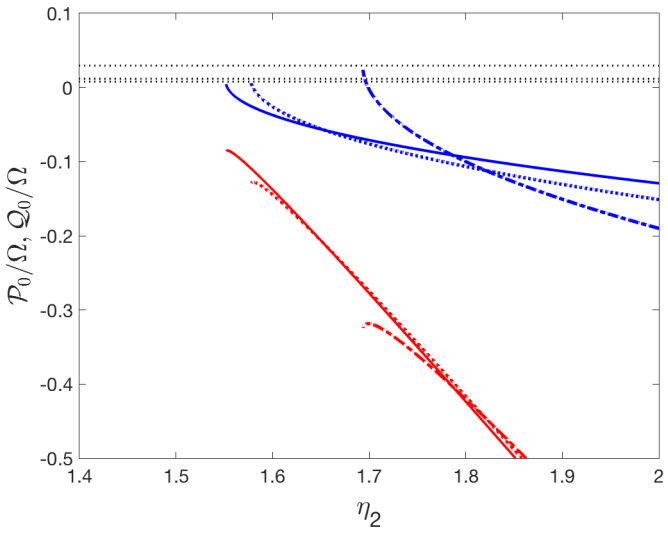

Figure 8: Graphs of P_0/Ω (blue) and Q_0/Ω (red) vs. η_2 for three different values of $\Omega = 30$ (solid line), $\Omega = 20$ (dotted line), and $\Omega = 8$ (dash-dotted line). Horizontal dotted black lines correspond to the critical value (3.26) of P_0 at which there is a loss of stability for P_0 and Q_0 as the equilibrium solution for (3.22).

Figure 7 indicates the source of the over-estimation by $\eta_{2\text{osc}}$ of the critical value for larger values of A/Ω or smaller values of Ω. The lower panels show results for $A\Omega^{-1} = 0.125$, corresponding to values in Figure 6 where the asymptotic approximation $\eta_{2\text{osc}}$ overestimates the advance of the critical value of η_2. In Figure 7 (Lower) we see that $\mathcal{V}, \mathcal{T}$ are not well approximated by (3.25), following from the fact that the separation of time scales used to get (3.25) is no longer valid for $\Omega = O(1)$ or smaller. For smaller values of η_2, where the oscillations cross Σ and in some cases also $\mathbf{S}$, the multiple scale approximation is not a good approximation for the piecewise-smooth continuous solutions, whose behavior is illustrated by the numerical solutions. For the smallest values of η_2, where $\eta_{\text{num}} < \eta_2 < \eta_{2\text{osc}}$, the multiple scale approximation predicts tipping and there is no approximation from (3.25) shown. However, the numerical calculations show attracting oscillations (such as the figure-of-eight solution in Figure 7) that cross both Σ and $\mathbf{S}$, without tipping to the temperature-dominate branch $\mathbf{N}$ for large $\mathcal{V}$. We expect that a separate local analysis for η_2 near η_{2c} is required to determine the tipping conditions for $\Omega = O(1)$ or smaller, which would involve constructing the piecewise-smooth solutions. We leave this analysis for a future treatment which makes full use of the geometry given by the piecewise-smooth structure [17].

4 High frequency oscillatory forcing combined with dynamic bifurcation

4.1 Overview

In this section we give the analytical approximation for the tipping point in the setting of dynamic NSF bifurcation, that is, with a bifurcation parameter slowly varying with rate $\epsilon \ll 1$, combined with high frequency forcing. $A > 0, \Omega \gg 1$. The analysis uses elements from both Section 2 with the slowly varying bifurcation parameter (only) and Section 3 with high frequency oscillatory forcing (only). Not only are these results helpful in designing the analytical approach, but we also see the competition between elements shifting the location of the tipping point: advances, observed in Section 3, and lags, observed Section 2. We again identify multiple scales analyses that are applied to both outer and inner expansions. As in the previous sections, we develop the approach first in the setting of a single DoF model and then adapt this for the Stommel model (1.5).

4.2 The single DoF model

We consider both $\epsilon \neq 0$ and $A \neq 0$ first in (2.1). In order to capture results for a range of high frequency Ω, with Ω^{-1} comparable to the rate ϵ for the slowly varying parameter μ, we introduce $\Omega = \epsilon^{-\lambda}$ for $\lambda > 0$. This framework allows us to incorporate the time scales both for the oscillations and for the slowly varying parameter μ, naturally leading to the choice of time scales $\tau = \epsilon t$ and $T = \epsilon^{-\lambda} t$. Using a multiple scales approximation for $x(\tau, T)$ in (2.1) yields

$$\begin{aligned} x_T + \epsilon^{\lambda+1} x_\tau =& \epsilon^\lambda(-\mu(\tau) + 2|x| - x|x| + A\sin(T)), \\ \mu_\tau(\tau) =& -1. \end{aligned} \tag{4.1}$$

As in the previous sections, we first consider an outer solution for $x < 0$ for $\mu > 0$, which points to a local expansion from which tipping is determined. Following the same procedures as in Section 3.2 together with a multiple scales approach, as shown in Appendix A.3 we obtain

$$x \sim 1 - \sqrt{1+\mu(t)} - \frac{\epsilon}{4(1+\mu(t))} - \epsilon^\lambda A\cos(\Omega t) + O(\epsilon^{1+\lambda}, \epsilon^{2\lambda}). \tag{4.2}$$

As in Section 3.2, we see that the outer expansion (4.2) fails for small μ, for which all three terms may be the same order. For example, taking $\mu = \epsilon m$, we write this condition in terms of A and ϵ

$$A \sim \epsilon^{1-\lambda} \frac{2m-1}{4}\,. \tag{4.3}$$

This condition suggests that two cases are of interest for the behavior of the tipping point, captured by the inner expansion: $\lambda \leq 1$ and $\lambda > 1$, which correspond respectively to cases with large or small values of A/Ω.

For the inner expansion we use a multiple scale expansion for $x(t,T)$, with slow and fast time scales t and $T = \epsilon^{-\lambda} t$, respectively, and $\mu = \epsilon m$. Then (2.1) takes the form

$$\begin{aligned} x_T + \epsilon^\lambda x_t &= -\epsilon^{\lambda+1} m(t) + \epsilon^\lambda 2|x| - \epsilon^\lambda x|x| + \epsilon^\lambda A \sin(T), \\ m_t(t) &= -1, \end{aligned} \tag{4.4}$$

which indicates that x must be scaled with a power of ϵ and its expansion must include a term with coefficient ϵ^λ. Then

$$x(t,T) = \epsilon^\lambda y_\lambda(t,T) + \epsilon^{q_1} y_1(t,T) + \ldots \epsilon^{q_2} y_2(t,T) + \ldots \tag{4.5}$$

with q_j depending on the value of λ and $q_1 < q_2$. With this form, it follows that $y_\lambda = -A\cos(T) + y_0(t)$, for both cases $\lambda \leq 1$ and $\lambda > 1$. Furthermore, it is straightforward to show that y_0 and y_1 have the same form up to a multiplicative constant, so we can drop y_0 without loss of generality.

4.2.1 Single DoF with $\Omega = \epsilon^{-\lambda}$, $\lambda \leq 1$:

Substituting (4.5) into (4.4) and balancing terms in order to obtain non-trivial solutions, we determine $q_1 = \lambda$, $q_2 = 2\lambda$. Then, collecting terms at successive powers of ϵ, we find that $y_\lambda = -A\cos(T)$, $y_{1T} = 0$ at $O(\epsilon^\lambda)$, and

$$O(\epsilon^{2\lambda}) : y_{2T} = -y_{1t} - \epsilon^{1-\lambda} m(t) + 2|y_1 - A\cos(T)|\,. \tag{4.6}$$

Applying the solvability condition (A.5) yields

$$y_{1t} = -\epsilon^{1-\lambda} m(t) + \frac{1}{\pi}\int_0^{2\pi} |y_1(t) - A\cos(T)|\, dT. \tag{4.7}$$

For $A < |y_1|$, this equation reduces to $y_{1_m} = -\epsilon^{1-\lambda} m - 2y_1$ for $y_1 < 0$, from which we recover a contribution similar to the term $1 - \sqrt{1+\mu}$ in (4.2) for $\mu \ll 1$. That is, we recover behavior similar to the outer solution in (4.2). For $A > |y_1|$, we evaluate the integral in (4.6) as in (3.7)-(3.9), treating y_1 as a constant relative to the fast time scale T,

$$y_{1t} \;=\; -\epsilon^{1-\lambda} m + \frac{4}{\pi}\left(\arcsin(y_1/A) y_1 + \sqrt{A^2 - y_1^2}\right)\,. \tag{4.8}$$

We wish to determine the critical tipping value of m (and μ), at which y_1 increases away from x_{eq}^-. However, in this case we don't get a closed form solution for y_1 from (4.8) since $m(t)$ is time-dependent. We use an approximation for (4.8) that allows us to get an explicit expression for the critical value of m corresponding to rapid growth in y_1. Since $|y_1| < A$ for tipping to occur, we expand the right hand side of (4.8) for $|y_1|/A \ll 1$, keeping up to quadratic terms. Also, it is convenient to use $m'(t) = -1$ to replace y_{1t},

$$y_{1_m} \approx \epsilon^{1-\lambda} m - \frac{4A}{\pi} - \frac{2}{\pi A} y_1^2. \tag{4.9}$$

The form (4.9) allows solutions in terms of Airy functions $Ai(z)$, as described in Appendix B. Then y_1 has the form

$$y_1(m) \sim \epsilon^{(1-\lambda)/3} \left(\frac{\pi A}{2}\right)^{2/3} \frac{\mathrm{Ai}'\left(\epsilon^{2(\lambda-1)/3}\left(\frac{2}{\pi A}\right)^{1/3}(\epsilon^{1-\lambda}m - \frac{4A}{\pi})\right)}{\mathrm{Ai}\left(\epsilon^{2(\lambda-1)/3}\left(\frac{2}{\pi A}\right)^{1/3}(\epsilon^{1-\lambda}m - \frac{4A}{\pi})\right)},$$

and x is given by

$$x(t) \sim \left[\epsilon^{(\lambda-1/2)}\frac{\pi A}{2}\right]^{2/3} \frac{\mathrm{Ai}'\left(\left(\frac{\Omega}{\epsilon^2}\right)^{1/3}\left(\frac{2}{\pi A}\right)^{1/3}(\mu(t) - \frac{4A}{\pi\Omega})\right)}{\mathrm{Ai}\left(\left(\frac{\Omega}{\epsilon^2}\right)^{1/3}\left(\frac{2}{\pi A}\right)^{1/3}(\mu(t) - \frac{4A}{\pi\Omega})\right)} - \frac{A}{\Omega}\cos(\Omega t) + \dots . \tag{4.10}$$

The singularity in (4.10) in terms of μ corresponds to the critical value for tipping, at which the solution increases away from x^-_{eq}. This critical value is given by the first root of the Airy function, yielding

$$\mu_{\mathrm{mixed}} = \left(\frac{\epsilon^2\pi A}{2\Omega}\right)^{1/3}\xi_r + \frac{4A}{\pi\Omega} = \left(\frac{\epsilon^2\pi A}{2\Omega}\right)^{1/3}\xi_r + \mu_{\mathrm{osc}}\,, \tag{4.11}$$

$$\mathrm{Ai}(\xi_r) = 0 \text{ for } \xi_r = -2.33811\dots . \tag{4.12}$$

As in the case of a smooth SNB, the tipping point is the sum of two contributions to the tipping point. One contribution (which is less than zero) corresponds to a lag in the tipping relative to the NSF point μ_c. This lag is due to slow variation of the parameter μ, similar to [8] but with a different parametric dependence. The second contribution $\mu_{\mathrm{osc}} > 0$ given in (3.10) corresponds to an advance in tipping due to the oscillations, as observed in Section 3.2 for static μ. Thus we have a competition between the factors that generate advance and lag in tipping, similar to that observed in [20] for variation near a smooth SNB.

Note that μ_{mixed} depends on the ratio A/Ω and on ϵ. For fixed ϵ, the advance described by μ_{osc} increases with decreasing $\lambda < 1$, or decreasing frequency Ω. Furthermore, we note that the result for μ_{mixed} is valid for $\lambda > 1/2$. For $\lambda \leq 1/2$, the asymptotic expansion (4.5) is no longer valid, since e.g. if $\lambda = 1/2$ then $q_2 = 2\lambda = 1$, and therefore we can not treat the quadratic terms as higher order, e.g. in (4.6). Note that decreasing λ corresponds to smaller frequency Ω, which can no longer be treated as high frequency, and a different approximation is required.

For $\lambda > 1$, a number of the steps used to obtain (4.6) are no longer valid, so an alternative expansion must be used. Related to this observation, complications can be seen from (4.11), from which we see that μ_{mixed} decreases and crosses zero for $A/\Omega \to O(\epsilon)$ for λ increasing beyond unity, corresponding to small A or large Ω. The case $\lambda > 1$ is discussed further below, where it is shown to be equivalent to the case of small A/Ω for λ near unity. Then a different approximation is needed to capture the dynamics of y_1 for all $\lambda > 1$.

4.2.2 Single DoF with $\Omega = \epsilon^{-\lambda}$, $\lambda > 1$:

We follow the same approach as for $\lambda < 1$, except we take $q_1 = 1$ in this case as follows from a standard balancing argument,

$$x(t,T) \sim -\epsilon^{\lambda} A\cos(T) + \epsilon y_1(t,T) + \epsilon^{q_2} y_2(t,T) + \dots . \tag{4.13}$$

Substituting (4.13) into (4.4) gives

$$O(\epsilon^{\lambda+1}): \qquad y_{2T} + \epsilon y_{1t} = -m(t) + 2|y_1 - \epsilon^{\lambda-1}A\cos(T)|\,, \tag{4.14}$$

taking $q_2 = \lambda + 1$.

Applying the solvability condition to (4.14) gives

$$y_{1t} = -\,m(t) + \frac{1}{\pi}\int_0^{2\pi} |y_1(t) - \epsilon^{\lambda-1} A\cos(T)|\, dT. \tag{4.15}$$

Note that this equation has the same form as (4.7) with a factor of $\epsilon^{\lambda-1}$ in front of A, due to the different choice for q_1. This indicates that for larger λ, Ω is larger and the influence of the oscillations is reduced. The same procedures as for $\lambda < 1$ above yields an equation of the form (4.8) with A replaced with $\epsilon^{\lambda-1}A$. However, the use of (4.8) is valid only for $\epsilon^\lambda A = A/\Omega > \epsilon y_1$, so that, for $A = O(1)$, the use of (4.8) is limited to values of $\lambda \gtrsim 1$. Note that this is consistent with the behavior of $\mu_{\rm mixed}$, which approaches and crosses zero for increasing Ω. Then for $\lambda > 1$, we must use a different approximation, recognizing that the critical value of μ is negative, for which the dynamics of x changes.

From (4.15) for y_1 and λ well above 1, the contribution from the oscillations are proportional to A/Ω, and thus a small perturbation. Therefore the tipping point is not advanced by the oscillations, as in the expression for $\mu_{\rm osc}$, and we expect the tipping point to correspond to $\mu < 0$. Then $m < 0$ and (4.15) takes the form $y_{1t} = -m(t) + 2|y_1|$ to leading order in ϵ, as in Section 2.2. Again, y_1 grows exponentially for $m < 0$ as observed in (2.9), yielding the approximation to the tipping point as $\mu_{\rm sv}$ from (2.11).

Figure 9 (UPPER) compares the tipping point computed from numerical simulations of the full model (2.1) for x with the two different results for critical μ; for $\lambda \le 1$, using $\mu_{\rm mixed}$ in (4.11) and for $\lambda > 1$ using $\mu_{\rm sv}$ in (2.11). As expected, the approximation (4.11) is appropriate for $\lambda < 1$. For $\lambda > 1$, the result asymptotes to the tipping point $\mu_{\rm sv}$, with slowly varying μ only, while (4.11) is not valid for $\lambda > 1$. Figure 9 (UPPER) also includes analogous asymptotic results for tipping for slow variation through the smooth SNB and oscillatory forcing, as described in (1.6) and analyzed in [20], with $z(0) > 0$ $\Omega = \epsilon^{-\lambda}$ and $\mathcal{A} = 1$. In that case the asymptotic approximation for the tipping value is $a_{\rm smooth}$ given in Table 1. The difference between the tipping location near the NSF bifurcation and that near the smooth SNB is dominated by the term that governs the lag: in the non-smooth case this term is $O(\epsilon \log \epsilon)$ while in the smooth case this term is $O(\epsilon^{2/3})$. Figure 9 (LOWER) shows simulations of x, illustrating tipping for the full system (2.1) for different values of λ, for the same values of A as in Figure 9 (UPPER). The solutions with $A = 2$ and different λ shown in red, green and magenta illustrate the effect of different forcing frequencies. In contrast, to illustrate the effect of different A, the red and blue solutions have the same λ but different amplitudes, $A = 2$ and $A = 5$ respectively. The analytical approximations for the tipping points $\mu_{\rm mixed}$ and $\mu_{\rm sv}$ are also shown for comparison.

We summarize the expressions for the tipping points of the NSF and SNB models in Table 1.

4.3 The Stommel model

To begin our analysis of the Stommel model in this case, we take our standard approach of tracking the solution near **F** for $\mathcal{V} < 0$ in (2.12) with both $\epsilon \ll 1$ and $A, B \sim O(1)$, that is,

$$\begin{aligned} \dot{\mathcal{V}} &= \eta_1 - \eta_2 - \mathcal{T} + \eta_3(\mathcal{T} - \mathcal{V}) + \mathcal{V}^2 + A\sin(\Omega t), \\ \dot{\mathcal{T}} &= \eta_1 - \mathcal{T}(1 - \mathcal{V}) + B\sin(\Omega t), \qquad \dot{\eta_2} = -\epsilon. \end{aligned} \tag{4.16}$$

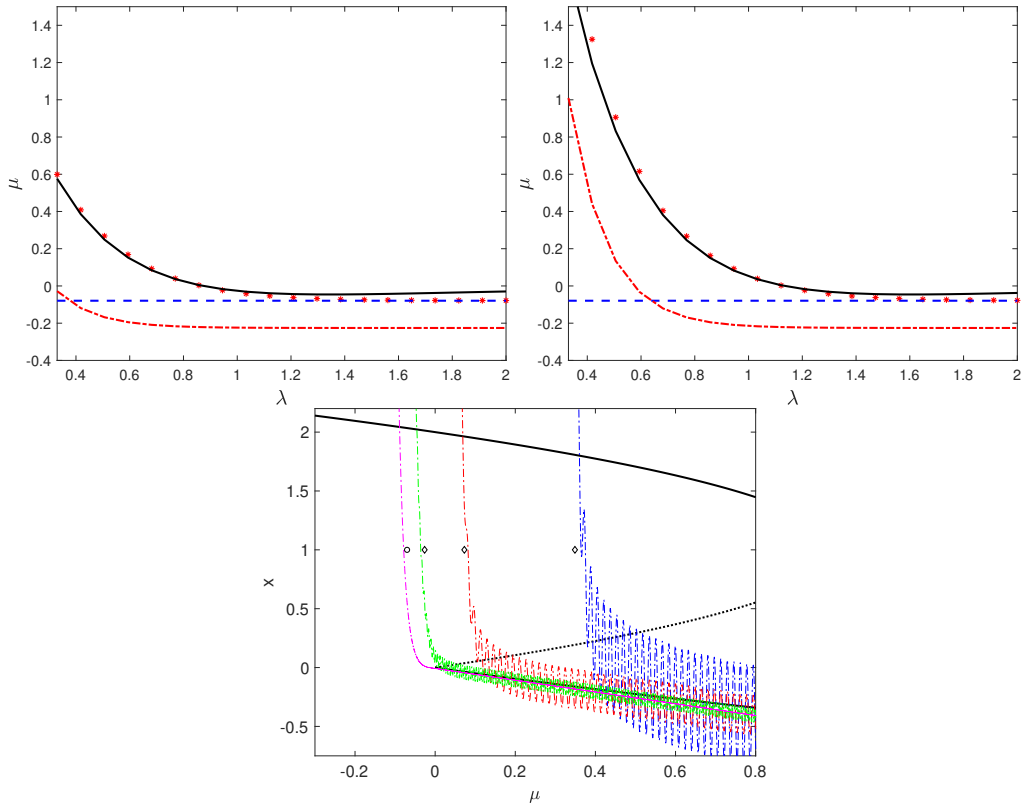

Figure 9: For all panels, $\epsilon = 0.03$. UPPER LEFT: For $A = 2$, comparison of the critical value μ_{mixed} (4.11) (black solid line), valid for $\lambda < 1$ and $\lambda \approx 1$, and the limiting critical value for $\lambda > 1$, μ_{sv} (2.11) (blue dotted line). Red stars indicate tipping in the numerical solution to (2.1), corresponding to the value of μ at which x reaches 1. The red dash-dotted line is the analogous result for the SNB (a_{smooth} in Table 1) analyzed in [20], shown for comparison. UPPER RIGHT: Similar to LEFT panel, but $A = 5$. LOWER: Simulations of the full system (2.1) for different combinations of frequency (in terms of λ) and amplitude superimposed on the static bifurcation curve (black lines), illustrating advanced tipping for larger A/Ω and delayed tipping for smaller A/Ω. Diamonds indicate analytical predictions μ_{mixed} for the tipping point in the three cases where $\lambda \leq 1$ (simulations of x in red and green for $A = 2$ and $\lambda = 0.7, 1.0$, respectively, and in blue for $A = 5$ and $\lambda = 0.7$), and the circle o indicates the analytical prediction μ_{sv}, (simulation of x in magenta for $A = 2$, $\lambda = 2$). The solutions with $A = 2$ and different λ shown in red, green and magenta illustrate the effect of different forcing frequencies, in contrast to the effect of different A, illustrated by the red and blue solutions with the same frequency ($\lambda = .7$) .

Tipping points for single DoF models: μ in (2.1) (NSF) and a in (1.6) (SNB)	
(NSF) Slowly varying μ only: $\epsilon \ll 1$, $A = 0$	$\mu_{\rm sv} = \epsilon \ln(\epsilon)/2 +$ corrections (2.11)
(NSF) High frequency oscillation only: $\epsilon = 0$, $A \neq 0$, $\Omega \gg 1$:	$\mu_{\rm osc} = \frac{4\|A\|}{\pi\Omega}$ (3.10)
(NSF) Slowly varying μ and high frequency oscillations: $\epsilon \ll 1$, $A \neq 0$, $\Omega = \epsilon^{-\lambda}$	(4.11)
$1/2 < \lambda \leq 1$:	$\mu_{\rm mixed} = \left(\frac{\epsilon^2 \pi A}{2\Omega}\right)^{1/3} \xi_r + \mu_{\rm osc}$
$\lambda > 1$:	$\mu_{\rm sv} = \epsilon \ln(\epsilon)/2 +$ corrections (2.11)
SNB: Slowly varying μ and high frequency oscillations: $\epsilon \ll 1$, $\mathcal{A} \neq 0$, $\Omega = \epsilon^{-\lambda}$	$a_{\rm smooth} = \epsilon^{2/3}\xi_r + \frac{\mathcal{A}^2}{2\Omega^2}$ [20]

Table 1: The value of the tipping point in the different cases for the single DoF models with NSF and smooth SNB for $\Omega \gg 1$.

As in Section 4.2, we take $\Omega = \epsilon^{-\lambda}$, for $\lambda > 0$ for high frequency. Using a standard multiple scales expansion with the slow time $\tau = \epsilon t$ and fast time $T = \epsilon^{-\lambda} t$, we construct an outer expansion,

$$\begin{aligned} \mathcal{V} \sim & \mathcal{V}_0 + \frac{\epsilon(\mathcal{V}_{0\tau}(1-\mathcal{V}_0) + (1-\eta_3)\mathcal{T}_{0\tau})}{(1-\eta_3)\mathcal{T}_0 + (2\mathcal{V}_0 - \eta_3)(1-\mathcal{V}_0)} - \epsilon^\lambda A\cos(\Omega t), \\ \mathcal{T} \sim & \mathcal{T}_0 + \frac{\epsilon \mathcal{T}_{0\tau}}{1-\mathcal{V}_0} - \frac{\epsilon \mathcal{T}_0(\mathcal{V}_{0\tau}(1-\mathcal{V}_0) + (1-\eta_3)\mathcal{T}_{0\tau})}{(1-\eta_3)\mathcal{T}_0(1-\mathcal{V}_0) + (2\mathcal{V}_0 - \eta_3)(1-\mathcal{V}_0)^2} - \epsilon^\lambda B\cos(\Omega t), \end{aligned} \tag{4.17}$$

where $\mathcal{V}_0$ and $\mathcal{T}_0$ are the quasi-equilibria identified for the slowly varying Stommel model in (2.16). As in (4.2), we see that the expansion (4.17) fails for $(\eta_2 - \eta_{2c}) \ll 1$, for which all three terms with coefficient ϵ^0, ϵ^1, and ϵ^λ may be of the same order. For example, taking $\eta_2 = \eta_{2c} + \epsilon\zeta$, we observe this failure for

$$A = O\left(\epsilon^{1-\lambda}\right), \qquad B = O\left(\epsilon^{1-\lambda}\right). \tag{4.18}$$

This condition suggests that two cases are of interest: for $\lambda \leq 1$ and $\lambda > 1$, which correspond respectively to the cases with small or larger values of $A/\Omega, B/\Omega$. For the inner expansion near the critical value $\eta_{2c} = \eta_1\eta_3$ we use a multiple scale approach with slow t and fast $T = \Omega t$ in (4.16), to get

$$\begin{aligned} \mathcal{V}_T + \epsilon^\lambda \mathcal{V}_t &= -\epsilon^{\lambda+1}\zeta + \epsilon^\lambda\left(\eta_1 - \mathcal{T} + \eta_3(\mathcal{T}-\mathcal{V}) + \mathcal{V}|\mathcal{V}| + A\sin(T)\right), \\ \mathcal{T}_T + \epsilon^\lambda \mathcal{T}_t &= \epsilon^\lambda\left(\eta_1 - \mathcal{T}(1-|\mathcal{V}|) + B\sin(T)\right), \\ \zeta_t &= -1, \qquad \eta_2(t) = \eta_{2c} + \epsilon\zeta(t). \end{aligned} \tag{4.19}$$

Analogous to (4.5), the form of (4.19) implies that $\mathcal{V}$ and $\mathcal{T}$ must be scaled with a power of ϵ near the critical value $(\mathcal{V}, \mathcal{T}) = (0, \eta_1)$ to obtain non-trivial results, and must include a term with coefficient ϵ^λ. We then use (4.19) together with the inner expansions,

$$\begin{aligned} \mathcal{V}(t,T) \sim & \epsilon^\lambda \mathcal{X}_\lambda(t,T) + \epsilon^{q_1}\mathcal{X}_1(t,T) + \epsilon^{q_2}\mathcal{X}_2(t,T) + \ldots, \\ \mathcal{T}(t,T) \sim & \eta_1 + \epsilon^\lambda \mathcal{Y}_\lambda(t,T) + \epsilon^{q_1}\mathcal{Y}_1(t,T) + \epsilon^{q_2}\mathcal{Y}_2(t,T) + \ldots, \end{aligned} \tag{4.20}$$

in the system for $\mathcal{V}$ and $\mathcal{T}$ (4.16). With this form it follows that

$$\mathcal{X}_\lambda = -A\cos(T) + \mathcal{X}_0(t), \qquad \mathcal{Y}_\lambda = -B\cos(T) + \mathcal{Y}_0(t)) \tag{4.21}$$

for both cases $\lambda \leq 1$ and $\lambda > 1$ considered below. As in Section 4.2, it is straightforward to show that $\mathcal{X}_0$ and $\mathcal{Y}_0$ have the same form as $\mathcal{X}_1$ and $\mathcal{Y}_1$, respectively, so without loss of generality we drop $\mathcal{X}_0$ and $\mathcal{Y}_0$.

4.3.1 The Stommel model with $\Omega = \epsilon^{-\lambda}$, $\lambda \leq 1$:

For $q_1 = \lambda$, $q_2 = 2\lambda$, and substituting (4.20) into (4.16) we obtain $\mathcal{X}_{1T} = 0$ and $\mathcal{Y}_{1T} = 0$ at $O(\epsilon^{\lambda})$, with the notation $\mathcal{X}_{jT} = \frac{\partial \mathcal{X}_j}{\partial T}$. Then at the next order,

$$O\left(\epsilon^{2\lambda}\right): \quad \begin{cases} \mathcal{X}_{2T} = & -\mathcal{X}_{1t} - \epsilon^{1-\lambda}\zeta(t) - \eta_3\mathcal{X}_1 - (1-\eta_3)\mathcal{Y}_1, \\ \mathcal{Y}_{2T} = & -\mathcal{Y}_{1t} - \eta_1|\mathcal{X}_1 - A\cos(T)| - \mathcal{Y}_1. \end{cases} \tag{4.22}$$

assuming that we follow the branch **F** where $\mathcal{X} < 0$ ($\mathcal{V} < 0$). Note that the result for (4.22) assumes that $\lambda > \frac{1}{2}$, so that quadratic terms appear in higher order corrections. Similar to Section 3.3 we apply the solvability condition as in (A.5) to (4.22) to get

$$\begin{aligned} \mathcal{X}_{1t} =& -\epsilon^{1-\lambda}\zeta(t) - \eta_3\mathcal{X}_1 - (1-\eta_3)\mathcal{Y}_1, \\ \mathcal{Y}_{1t} =& -\frac{\eta_1}{2\pi}\int_0^{2\pi} |\mathcal{X}_1(t) - A\cos(T)|\, dT - \mathcal{Y}_1, \\ \zeta_t =& -1. \end{aligned} \tag{4.23}$$

For $|\mathcal{X}_1(t)| > A$ we recover the behavior of the outer solution, as in (4.20) . For $|\mathcal{X}_1(t)| \leq A$, the term $\mathcal{X}_1(t) - A\cos(T)$ in (4.23) changes sign. Then we evaluate the integral in (4.23) as in (3.20),

$$\begin{aligned} \mathcal{X}_{1t} =& -\epsilon^{1-\lambda}\zeta(t) - \eta_3\mathcal{X}_1(s) - (1-\eta_3)\mathcal{Y}_1 \\ \mathcal{Y}_{1t} =& -\frac{2\eta_1}{\pi}\left(\arcsin(\mathcal{X}_1/A)\mathcal{X}_1 + \sqrt{A^2 - \mathcal{X}_1^2}\right) - \mathcal{Y}_1\,. \end{aligned} \tag{4.24}$$

To identify the tipping point, we get an analytically explicit form from which we identify rapid growth in $\mathcal{X}$. Using a Taylor expansion for $\mathcal{X}_1/A \ll 1$ as in (4.8)-(4.9), and using $\zeta_t = -1$ to replace $\mathcal{X}_{1t}$ with $-\mathcal{X}_{1\zeta}$, we get

$$\begin{aligned} \mathcal{X}_{1\zeta} =& \epsilon^{1-\lambda}\zeta + \eta_3\mathcal{X}_1 + (1-\eta_3)\mathcal{Y}_1 \\ \mathcal{Y}_{1\zeta} =& \frac{2\eta_1 A}{\pi} + \frac{\eta_1}{\pi A}\mathcal{X}_1^2 + \mathcal{Y}_1\,. \end{aligned} \tag{4.25}$$

As in Section 3.3, growth is driven primarily by shifts in $\mathcal{X}_1$, with $\mathcal{Y}_1$ following accordingly. Then we neglect $\mathcal{Y}_{1t}$ in (4.24) -(4.25), which yields the quasi-steady approximation,

$$\mathcal{Y}_1 = -\frac{2\eta_1}{\pi}\left(\arcsin(\mathcal{X}_1/A)\mathcal{X}_1 + \sqrt{A^2 - \mathcal{X}_1^2}\right) \approx -\frac{2\eta_1 A}{\pi} - \frac{\eta_1}{\pi A}\mathcal{X}_1^2\,. \tag{4.26}$$

Substituting (4.26) in (4.25) then yields the non-autonomous equation for $\mathcal{X}_1$

$$\mathcal{X}_{1\zeta} = \epsilon^{1-\lambda}\zeta - \frac{2\eta_1(1-\eta_3)A}{\pi} + \eta_3\mathcal{X}_1 - \frac{\eta_1(1-\eta_3)}{\pi A}\mathcal{X}_1^2. \tag{4.27}$$

Now (4.27) is in the form of (B.2), from which we identify the tipping point, as we did in (4.10) -(4.11),

$$\zeta_{\text{mixed}} = \left(\frac{\epsilon^{(\lambda-1)}\pi A}{\eta_1(1-\eta_3)}\right)^{1/3}\xi_r + \epsilon^{\lambda-1}\frac{\eta_1(1-\eta_3)A}{\pi}\left(2 - \left(\frac{\pi\eta_3}{2\eta_1(1-\eta_3)}\right)^2\right) \implies \tag{4.28}$$

$$\eta_{2\text{mixed}} \approx \left(\frac{\epsilon^2\pi A}{\eta_1(1-\eta_3)\Omega}\right)^{1/3}\xi_r + \eta_{2\text{osc}}\,, \tag{4.29}$$

for ξ_r given in (4.11). Note that the second term in ζ_{mixed} is the Taylor expansion of ζ_{osc} (3.24) for $\eta_3/[\eta_1(1-\eta_3)] \ll 1$, leading to (4.29). The form of $\eta_{2\text{mixed}}$ is similar to that of μ_{mixed} in (4.11), that is, having a term corresponding to an advance of tipping in $\eta_{2\text{osc}}$ and another term corresponding to a lag in tipping, which involves the root of an Airy function. Recall that this result is valid for $\lambda > 1/2$, for which we have neglected quadratic terms in the equation for the corrections (4.22).

4.3.2 The Stommel model with $\Omega = \epsilon^{-\lambda}$, $\lambda > 1$.

Similar to the single DoF case, we start with the expansions

$$\begin{aligned} \mathcal{V}(t,T) &\sim -\epsilon^{\lambda} A\cos(T) + \epsilon\mathcal{X}_1(t,T) + \epsilon^{q_2}\mathcal{X}_2(t,T) + \dots \\ \mathcal{T}(t,T) &\sim -\epsilon^{\lambda} B\cos(T) + \epsilon\mathcal{X}_1(t,T) + \epsilon^{q_2}\mathcal{Y}_2(t,T) + \dots \end{aligned} \tag{4.30}$$

As in Section 4.2.1, here we take $q_1 = 1$ and $q_2 = \lambda+1$. Substituting (4.30) into (4.16) and collecting coefficients at each order of ϵ, we find at $O(\epsilon)$ that $\mathcal{X}_{1T} = 0, \mathcal{Y}_{1T} = 0$ and

$$O(\epsilon^{\lambda+1}): \begin{cases} \mathcal{X}_{2T} + \mathcal{X}_{1t} = & -\zeta(t) - \eta_3\mathcal{X}_1 - (1-\eta_3)\mathcal{Y}_1, \\ \mathcal{Y}_{2T} + \mathcal{Y}_{1t} = & -\eta_1|\mathcal{X}_1 - \epsilon^{\lambda-1}A\cos(T)| - \mathcal{Y}_1\,. \end{cases} \tag{4.31}$$

Applying the solvability condition (A.5) to (4.31) then gives

$$\begin{aligned} \mathcal{X}_{1t} &= -\zeta(t) - \eta_3\mathcal{X}_1 - (1-\eta_3)\mathcal{Y}_1, \\ \mathcal{Y}_{1t} &= -\frac{\eta_1}{2\pi}\int_0^{2\pi} |\mathcal{X}_1(t) - \epsilon^{\lambda-1}A\cos(T)|\,dT - \mathcal{Y}_1\,. \\ \zeta_t &= -1. \end{aligned} \tag{4.32}$$

This equation has the same form as (4.23) with a factor of $\epsilon^{\lambda-1}$ in front of A, due to the different choice for q_1. Once again, for larger λ, Ω is larger and the influence of the oscillations is reduced. Evaluating the integral, and using the same approach as for $\lambda < 1$ yields (4.24) with A replaced with $\epsilon^{\lambda-1}A$. Recall that the results such as those obtained in (4.23)-(4.25) are valid only for $\epsilon^{\lambda}A = A/\Omega > \epsilon\mathcal{X}_1$, so that, for $A = O(1)$, the use of (4.32) is limited to values of $\lambda \gtrsim 1$. This is consistent with the behavior of $\eta_{2\text{mixed}}$ in (4.28), which decreases and crosses η_{2c} for $A/\Omega \to O(\epsilon)$. Then for $\lambda > 1$, we must use a different approximation, recognizing that the critical value satisfies $\eta_2 < \eta_{2c}$ ($\zeta < 0$), for which the dynamics of $\mathcal{X}$ and $\mathcal{Y}$ change.

For $\lambda > 1$, the contribution from the oscillations is proportional to A/Ω, and thus a small perturbation. Therefore the tipping point is not advanced by the oscillations, as in the expression for $\eta_{2\text{osc}}$, and we expect the tipping point to correspond to $\zeta < 0$. Equation (4.32) then takes the form of (2.20). Then there is exponentially fast growth of the solution for $\eta_2 < \eta_{2c}$ as observed in Section 2.3, yielding the approximation to the tipping point as $\eta_{2\text{sv}}$ from (2.25).

Figure 10 compares the results for $\eta_{2\text{mixed}}$ and $\eta_{2\text{sv}}$ to the tipping point obtained from (2.12). This illustrates the different behavior of the tipping point for the two cases of $\lambda \leq 1$, corresponding to smaller Ω or larger $A\Omega^{-1}$, and $\lambda > 1$ corresponding to $\Omega \gg 1$. Table 2 summarizes the different values of the tipping points and critical values of η_2 for the three different cases.

5 Summary and Future Work

Using a combination of local and multiple-scale analyses, we provide expressions for the tipping points near a NSF bifurcation in three settings. For the slowly varying bifurcation parameter of "rate" ϵ only, there is a lag for the dynamic bifurcation relative to the static NSF. The functional dependence on the rate parameter ϵ is $O(\epsilon\log\epsilon)$, in contrast to $\epsilon^{2/3}$ in the case of the smooth SNB as (1.6). For high frequency oscillatory forcing without the slowly varying bifurcation, there is an advance in the transition away from the branch of equilibria that terminates in the NSF, where that advance depends linearly on the amplitude-to-frequency ratio (A/Ω) of the oscillations. With high frequency forcing, an averaging approach based on multiple scales is applied. The nonlinearities then generate additional contributions to the averaged behavior, shifting the tipping point. For combined slowly varying bifurcation parameter and high frequency oscillatory forcing,

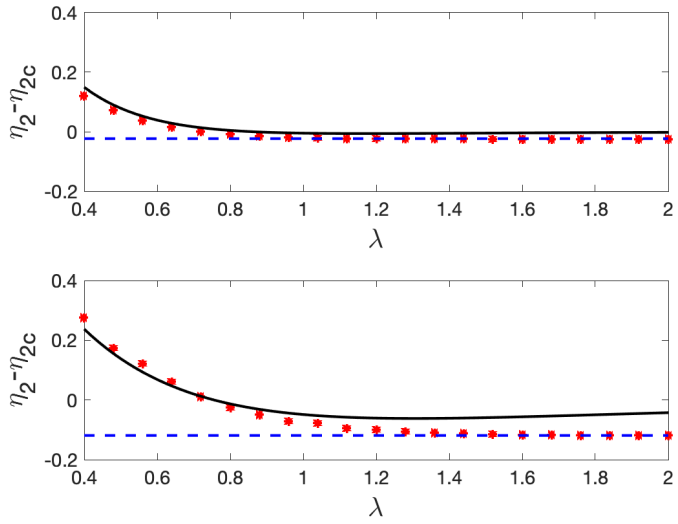

Figure 10: Comparison of the critical value $\eta_{2\text{mixed}}$ (black solid line) valid for $\lambda \lesssim 1$ and the limiting critical value $\eta_{2\text{slow}}$ for large λ (blue dotted line). Red stars indicate tipping in the numerical solution to (2.12), corresponding to the value of $\eta_2 - \eta_{2c}$ at which $\mathcal{V}$ reaches the cut-off, $v = 0.3$. Upper: $\epsilon = 0.005$. Lower $\epsilon = 0.05$. Other parameters: $\eta_1 = 4$,$\eta_3 = 3/8$, $A = 1$.

Tipping for the Stommel model with $\Omega \gg 1$ and η_2 slowly varying	
Slowly varying η_2 only: $\epsilon \ll 1$, $A = B = 0$	$\eta_{2\text{sv}} \sim \eta_{2c} - \frac{\epsilon}{\lambda_1} \log \epsilon$ + corrections (2.25)
High frequency oscillation only: $\epsilon = 0$, $A \neq 0$, $\Omega \gg 1$:	$\eta_{2\text{osc}} = \eta_1\eta_3 +$ $\frac{2(1-\eta_3)\eta_1}{\Omega\pi} A \cos\left(\frac{\eta_3\pi}{2(1-\eta_3)\eta_1}\right)$ (3.24)
Slowly varying η_2 and $\Omega \gg 1$ $\epsilon \ll 1$, $A \neq 0$, $\Omega = \epsilon^{-\lambda}$ $1/2 < \lambda \leq 1$: $\lambda > 1$:	 $\eta_{2\text{mixed}} \approx \left(\frac{\epsilon^2\pi A}{\eta_1(1-\eta_3)\Omega}\right)^{1/3} \xi_r + \eta_{2\text{osc}}$ (4.28) $\eta_{2\text{sv}} \sim \eta_{2c} - \frac{\epsilon}{\lambda_1} \log \epsilon$ + corrections (2.25)

Table 2: The asymptotic approximations for tipping values and critical values of η_2 for different cases.

there is a more complex functional dependence on all parameters involved, capturing a competition between lag and advance of the tipping point. The competition is observed directly in the analytical expressions for the tipping points, where there is a change in the leading order term that gives the location of the tipping. We relate this change to the magnitude of the amplitude-to-frequency ratio, A/Ω, which characterizes the size of the oscillations in the solution. Writing Ω in terms of the rate parameter $\Omega = \epsilon^{-\lambda}$, the dominant parameter dependence of the tipping point is different for the two ranges $1/2 < \lambda \leq 1$ and $\lambda > 1$, assuming $A = O(1)$. Expressing this difference in terms of A/Ω, for large values the oscillation-driven advance dominates the tipping behavior, while for small A/Ω, the tipping value asymptotes to the lag of the dynamic bifurcation. Detailed quantitative comparisons are provided in Section 4.2 for the tipping point behavior near the NSF vs. the results for a SNB as in (1.6).

The methods for a NSF are developed in a single DoF model, and the approaches are then adapted for the two DoF Stommel model in (1.5) with slowly varying fresh water forcing parameter η_2 and oscillatory forcing. In the case of high frequency forcing, we show that the tipping behavior for the Stommel model near η_{2c} is remarkably similar to that of the single DoF model, again for three cases: (i) η_2 is slowly varying only, without oscillations in η_1 or η_2 ($A = B = 0$), (ii) η_1 and η_2 have high frequency oscillations $\Omega \gg 1$, without slow variation $\epsilon = 0$; and (iii) there is both slow variation and high frequency oscillation, with A, B, and ϵ all non-zero in (1.5). The direct application of the method used in the single DoF case follows from a linear analysis near η_{2c}, indicating that when forced by high frequency oscillations, the transition is primarily driven by fluctuations in $\mathcal{V}$, with $\mathcal{T}$ essentially slaved to $\mathcal{V}$. Then we approximate $\mathcal{T}$ with a quasi-static approximation, leaving the calculation of the tipping point in terms of a reduced problem similar to that given in the single DoF system. This approximation allows us to avoid the construction of piecewise-smooth continuous solutions for $\mathcal{V}$ and $\mathcal{T}$ near η_{2c} in the high frequency case. Such constructions are necessary for frequencies that are O(1) and smaller. However the analysis in the high frequency case is simplified by the observation that as the focus and the saddle in the Stommel model approach the NSF, the linearisation of the system about them changes very little (in stark contrast to the SNB case). Thus the whole system can be studied locally by looking at the coalescence of two linear systems separated by Σ. We leave this calculation for $O(1)$ forcing frequency for future work. The linear analysis that provides the basis for this reduction is discussed in Section 3.4. Understanding the limitations of the approximation for the high frequency cases used in this study, we can also track the validity of the approximations for the tipping point over relevant frequency ranges and indicate parameter ranges for which a fully 2D approximation is needed.

Acknowledgments: This research was supported in part by a NSERC Discovery Accelerator Grant, a Simons Foundation Fellowship, and the Isaac Newton Institute for Mathematical Sciences. The authors are grateful for helpful discussions during the 2016 Climate Modeling Workshop at the Centre de Recerca Matemàtica (CRM), part the Intensive Research Program *Advances in Nonsmooth Dynamics*.

References

[1] Richard B Alley, Jochem Marotzke, William D Nordhaus, Jonathan T Overpeck, Dorothy M Peteet, Roger A Pielke, RT Pierrehumbert, PB Rhines, TF Stocker, LD Talley, et al. Abrupt climate change. *Science*, 299(5615):2005–2010, 2003.

[2] Alain Bensoussan, Jacques-Louis Lions, and George Papanicolaou. *Asymptotic analysis for periodic structures*, volume 374. American Mathematical Soc., 2011.

[3] Mario Bernardo, Chris Budd, Alan Richard Champneys, and Piotr Kowalczyk. *Piecewise-smooth dynamical systems: theory and applications*, volume 163. Springer Science & Business Media, 2008.

[4] Levke Caesar, Stefan Rahmstorf, Alexander Robinson, Georg Feulner, and V Saba. Observed fingerprint of a weakening atlantic ocean overturning circulation. *Nature*, 556(1):191–196, 2018.

[5] Henk A Dijkstra. *Nonlinear climate dynamics*. Cambridge University Press, 2013.

[6] T Erneux and JP Laplante. Jump transition due to a time-dependent bifurcation parameter in the bistable ioadate–arsenous acid reaction. *The Journal of Chemical Physics*, 90(11):6129–6134, 1989.

[7] K. Gowda and C. Kuehn. Warning signs for pattern-formation in spdes. *Communications in Nonlinear Science and Numerical Simulation*, 22:55–69, 2015.

[8] Richard Haberman. Slowly varying jump and transition phenomena associated with algebraic bifurcation problems. *SIAM Journal on Applied Mathematics*, 37(1):69–106, 1979.

[9] S. Hottovy and S.N. Stechmann. Threshold models for rainfall and convection: Deterministic versus stochastic triggers. *SIAM Journal on Applied Mathematics*, 75(2):861–884, 2015.

[10] Timothy Lenton. Early warning of climate tipping points. *Nature Climate Change*, 1:201–209, 2011.

[11] Jochem Marotzke. Abrupt climate change and thermohaline circulation: Mechanisms and predictability. *Proceedings of the National Academy of Sciences*, 97(4):1347–1350, 2000.

[12] Kgomotso Morupisi and Chris Budd. An analysis of the periodically forced PP04 climate model, using the theory of non-smooth dynamical systems. *IMA Journal of Applied Mathematics*, 2020.

[13] Didier Paillard and Frédéric Parrenin. The antarctic ice sheet and the triggering of deglaciations. *Earth and Planetary Science Letters*, 227(3-4):263–271, 2004.

[14] Stefan Rahmstorf. The thermohaline ocean circulation: A system with dangerous thresholds? *Climatic Change*, 46(3):247–256, 2000.

[15] Stefan Rahmstorf. Ocean circulation and climate during the past 120,000 years. *Nature*, 419(6903):207–214, 2002.

[16] Nestor E Sanchez. The method of multiple scales: asymptotic solutions and normal forms for nonlinear oscillatory problems. *Journal of Symbolic Computation*, 21(2):245–252, 1996.

[17] David John Warwick Simpson. *Bifurcations in piecewise-smooth continuous systems*, volume 70. World Scientific, 2010.

[18] Henry Stommel. Thermohaline convection with two stable regimes of flow. *Tellus*, 13(2):224–230, 1961.

[19] James Walsh, Esther Widiasih, Jonathan Hahn, and Richard McGehee. Periodic orbits for a discontinuous vector field arising from a conceptual model of glacial cycles. *Nonlinearity*, 29:1843, 2016.

[20] Jielin Zhu, Rachel Kuske, and Thomas Erneux. Tipping points near a delayed saddle node bifurcation with periodic forcing. *SIAM Journal on Applied Dynamical Systems*, 14(4):2030–2068, 2015.

A Appendices

A.1 Dynamic bifurcation for the Stommel model

To complete the expression for $\mathcal{V}$ in (2.23), we find the constant K_{11}, using a quasi-steady approximation for $\mathcal{V} \sim \mathcal{V}_0 + \epsilon\mathcal{V}_1$ for $\mathcal{V} < 0$. First, $\mathcal{V}_0$ and $\mathcal{T}_0$ are given by (2.16), and the correction $\mathcal{V}_1$ follows from solving (2.15), with $\mathcal{V}_{0\tau}$ and $\mathcal{T}_{0\tau}$ obtained by differentiating (2.16) and using $\eta_{2\tau} = -1$. Then

$$\mathcal{V}_1 = -\frac{1 + \eta_3\eta_1 - \eta_1}{[(\eta_3 - 1)\eta_1/(1 - \mathcal{V}_0^2)^2 - \eta_3 + 2\mathcal{V}_0]^2}\,. \tag{A.1}$$

Similar to (2.8)-(2.9), the expression for $\mathcal{V} < 0$ provides the value of η_2 at which $\mathcal{V}(\eta_2) = 0$, and thus also the initial condition for $\mathcal{V} > 0$ from which to determine K_{11} in (2.23).

A.2 High Frequency Oscillatory Forcing: outer solutions

A.2.1 The single DoF model

As noted in Section 3.2 we provide steps to obtain a formal multiple scales approximation of the outer solution of the nonlinear equation (3.1) for $x < 0$. While not critical for the results for this case, these steps illustrate the approach used also in later sections. The expansion is based on a slow time t and fast time $T = \Omega t$ for $\Omega \gg 1$,

$$x(t,T) \sim x_0(t,T) + \Omega^{-1}x_1(t,T) + \Omega^{-2}x_2(t,T) + O(\Omega^{-3}). \tag{A.2}$$

Substituting (A.2) in (2.1), together with the multiple scales treatment of the time derivative, $\dot{x} \to x_t + \Omega^{-1}x_T$, yields a sequence of equations by collecting terms with like coefficients Ω^{-j}. The $O(1)$ equation $x_{0T} = 0$ indicates that $x_0 = x_0(t)$. Then the next order equations are

$$O(\Omega^{-1}): \quad x_{1T} = -x_{0t} - \mu - 2x_0 + x_0^2 + A\sin(T) \equiv R_1(t,T)\,. \tag{A.3}$$

$$O(\Omega^{-2}): \quad x_{2T} + x_{1t} = -2x_1 + 2x_0x_1 \equiv R_2(t,T)\,. \tag{A.4}$$

To ensure that x_1 and x_2 do not include secular terms that grow in time, the right hand sides of (A.3)-(A.4) must satisfy a solvability condition [2],

$$\frac{1}{2\pi}\int_0^{2\pi} R_i(t,T)\,dT = 0\,. \tag{A.5}$$

Applying (A.5) in the multiple scales context, the $O(1)$ time scale t is treated as a constant relative to the fast time T. Then we obtain the following equations for $x_0(t)$ and $x_1(T,t)$, for $x_0 < 0$,

$$\begin{aligned} x_{0t} = -\mu - 2x_0 + x_0^2 \implies x_0 &= 1 - \sqrt{1+\mu} \\ x_{1T} = A\sin(T) \implies x_1(t,T) &= v_1(t) - A\cos(T). \end{aligned} \tag{A.6}$$

Substituting (A.6) and applying (A.5) to R_2 in (A.4), yields

$$v_{1t} = -2\sqrt{1+\mu}\,v_1 \tag{A.7}$$

Noting that $v_1 \to 0$ as $t \to \infty$ for $\mu > 0$, we then obtain (3.1) as the attracting solution near $x_{\rm eq}^-$.

A.2.2 The Stommel model

Following the approach in Appendix A.2.1, we substitute into (1.5) the multiple scales expansions for $\mathcal{V}$ and $\mathcal{T}$ analogous to (A.2). We seek the attracting solution for $\mathcal{V} < 0$ near the lower branch **F** away from η_{2c}. Collecting coefficients of powers of Ω^{-1}, the $O(1)$ terms are $\mathcal{V}_{0T} = \mathcal{T}_{0T} = 0$, and

$$O(\Omega^{-1}): \quad \begin{cases} \mathcal{V}_{1T} = & -\mathcal{V}_{0t} + \eta_1 - \eta_2 + \eta_3(\mathcal{T}_0 - \mathcal{V}_0) - \mathcal{T}_0 + \mathcal{V}_0^2 + A\sin(T), \\ \mathcal{T}_{1T} = & -\mathcal{T}_{0t} + \eta_1 - \mathcal{T}_0(1 - \mathcal{V}_0) + B\sin(T)\,. \end{cases} \tag{A.8}$$

Applying a solvability condition similar to (A.5) to (A.8), we find that the equations for $\mathcal{V}_0$ and $\mathcal{T}_0$ are (2.12) with fixed η_2 and $A = B = 0$. Then for large t, $\mathcal{V}_0$ and $\mathcal{T}_0$ approach the stable equilibrium on the lower branch **F**. Then solving (A.8) yields

$$\begin{pmatrix} \mathcal{V}_1 \\ \mathcal{T}_1 \end{pmatrix} = -\begin{pmatrix} A \\ B \end{pmatrix}\cos(T) + \begin{pmatrix} \mathcal{V}_{11}(t) \\ \mathcal{T}_{11}(t) \end{pmatrix}, \tag{A.9}$$

where one can show that $\mathcal{V}_{11}(t) \to 0,\ \mathcal{T}_{11}(t) \to 0$ for large t. Then the behavior near **F** away from η_{2c} is given by (3.14).

A.3 Slow Variation and Oscillatory Forcing: the single DoF model

The form of (4.1) suggests a multiple scales expansion that includes both integer powers of ϵ and ϵ^λ

$$x(\tau, T) \sim x_0(\tau, T) + \epsilon^\lambda x_1(\tau, T) + \max(\epsilon^{1+\lambda}, \epsilon^{2\lambda})x_2 + \dots. \tag{A.10}$$

Depending on whether λ is less than or greater than 1, the higher order correction may be $O(\epsilon^{\lambda+1})$ or $O(\epsilon^{2\lambda})$. For concreteness we take $\lambda < 1$ in the steps below, noting that $\lambda > 1$ yields the same results for x_0 and x_1. Note that here we take $\lambda > 1/2$ as discussed in the main text. Substituting (A.10) into (4.1) gives a sequence of equations at each order of ϵ, with $x_{0T} = 0$ implying that $x_0 = x_0(\tau)$, and

$$O(\epsilon^\lambda): \quad x_{1T} = -\mu(\tau) - 2x_0 + x_0^2 + A\sin(T), \tag{A.11}$$

$$O(\epsilon^{2\lambda}): \quad x_{2T} = -\epsilon^{1-\lambda}x_{0\tau} - 2x_1 + 2x_0x_1. \tag{A.12}$$

Applying the solvability condition (A.5) to (A.11) and (A.12) we find x_0 and x_1 as follows,

$$\begin{aligned} 0 =& -\mu(\tau) - 2x_0(\tau) + x_0^2(\tau), \implies x_0(\tau) = 1 - \sqrt{1 + \mu(\tau)}, \text{ then} \\ x_{1T} =& A\sin(T) \implies x_1 = v_1(\tau) - A\cos(T), \text{ and} \\ 0 =& -\epsilon^{1-\lambda}x_{0\tau} - 2v_1 + 2\left(1 - \sqrt{1 + \mu(\tau)}\right)v_1 \implies v_1(\tau) = -\epsilon^{1-\lambda}\frac{x_{0\tau}}{2\sqrt{1 + \mu(\tau)}}. \end{aligned} \tag{A.13}$$

using $\mu_\tau = -1$. Combining results yields the outer expansion (4.2).

B General results for non-autonomous ODEs with quadratic nonlinearity

We use results from [8] for the general single DoF ODE with a quadratic nonlinearity and a dynamic bifurcation near a saddle node bifurcation,

$$\begin{aligned} \dot{x} =& Da + k_0 + k_1x + k_2x^2, \\ \dot{a} =& -\epsilon, \end{aligned} \tag{B.1}$$

where $\epsilon \ll 1$. Systems of this form appear in many physical problems like Erneux [6] and [20]. Following the approach of [8], where x and a are rescaled with $\epsilon^{1/3}$ and $\epsilon^{2/3}$, and x_t is rewritten in terms of x_a, the tipping point for x is obtained in terms of a singularity corresponding to the first zero of the Airy function, $\mathbf{Ai}(\xi_r) = 0$. Specifically, the tipping point is then

$$a_{\text{tip}} = \left(\frac{\epsilon^2}{D|k_2|}\right)^{1/3} \xi_r - \frac{a_s}{D} \quad \text{for} \quad a_s = k_0 + \frac{k_1^2}{4|k_2|}, \tag{B.2}$$

Detailed calculations are provided in [20].